The Islamic University–Gaza

Research and Postgraduate Affairs

Faculty of Science

Department of Physics

الجـامعــــــة الإســــلاميــة ــ غـزة

شئون البحث العلمي والدراسات العليا

كليـــــة العلـــــــــــــــــوم

ماجستير الفيزيـــــــــــاء

Effect of Adding Nano Layers on the Performance of Solar Cells Sensitized with Eosin Y and its Derivatives

تأثير إضافة طبقات نانوية على أداء الخلايا الشمسية المحفزة باستخدام إيوسين (Y) ومشتقاته

Dalal A. Hashem

Supervised by

Dr. Taher M. El-Agez

Associate Professor of Physics

Dr. Sofyan A. Taya

Associate Professor of Physics

A thesis submitted in partial fulfilment
of the requirements for the degree of
Master of Science in Physics

February, 2017

<div dir="rtl">

إقــــرار

أنا الموقع أدناه مقدم الرسالة التي تحمل العنوان:

</div>

Effect of Adding Nano Layers on the Performance of Solar Cells Sensitized with Eosin Y and its Derivatives
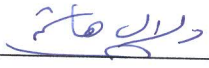
<div dir="rtl">

تأثير إضافة طبقات نانوية على أداء الخلايا الشمسية المحفزة باستخدام إيوسين(Y) ومشتقاته

أقر بأن ما اشتملت عليه هذه الرسالة إنما هو نتاج جهدي الخاص، باستثناء ما تمت الإشارة إليه حيثما ورد، وأن هذه الرسالة ككل أو أي جزء منها لم يقدم من قبل الاخرين لنيل درجة أو لقب علمي أو بحثي لدى أي مؤسسة تعليمية أو بحثية أخرى.

</div>

Declaration

I understand the nature of plagiarism, and I am aware of the University's policy on this.

The work provided in this thesis, unless otherwise referenced, is the researcher's own work, and has not been submitted by others elsewhere for any other degree or qualification.

Student's name:	دلال عبدالرؤوف أحمد هاشم	اسم الطالب:
Signature:	دلال هاشم	التوقيع:
Date:	19/4/2017	التاريخ:

بِسْمِ اللَّهِ الرَّحْمَنِ الرَّحِيمِ

الجامعة الإسلامية-غزة

The Islamic University of Gaza

Ref:	الرقم: ج س غ/35/
Date:	التاريخ: 29/03/2017

نتيجة الحكم على أطروحة ماجستير

بناءً على موافقة شئون البحث العلمي والدراسات العليا بالجامعة الإسلامية بغزة على تشكيل لجنة الحكم على أطروحة الباحثـة/ دلال عبدالرؤوف احمد هاشـم لنيـل درجـة الماجسـتير فـي كليـة *العلـوم* قسم *الفيزياء* وموضوعها:

تأثير إضافة طبقات نانوية على أداء الخلايا الشمسية المحفزة باستخدام إيوسين Y ومشتقاته

Effect of adding nano layers on the performance of solar cells sensitized with eosin Y and it's derivatives

وبعد المناقشة العلنية التي تمت اليوم الأربعاء 01 رجب 1438هـ، الموافق 2017/03/29م الساعة التاسعة والنصف صباحاً بمبني اللحيدان، اجتمعت لجنة الحكم على الأطروحة والمكونة من:

د. سفيان عبـد الـرحمن تايـه	مشـرفاً و رئيسـاً	....
د. طـاهر محمـد العـاجز	مشــــرفاً	....
د. حسـين عبـد الكـريم داوود	مناقشـاً داخليـاً	....
أ.د. أحمــد أسـعد التيـان	مناقشـاً خارجيـاً	....

وبعد المداولة أوصت اللجنة بمنح الباحثة درجة الماجستير في كلية العلوم/ قسم الفيزياء.

واللجنة إذ تمنحها هذه الدرجة فإنها توصيها بتقوى الله ولزوم طاعته وأن تسخر علمها في خدمة دينها ووطنها.

والله ولي التوفيق،،،

نائب الرئيس لشئون البحث العلمي والدراسات العليا

أ.د. عبدالرؤوف علي المناعمة

Abstract

Dye sensitized solar cells (DSSCs) is a new technology which considered to be the third generation of the photovoltaic technology. DSSCs have multiple advantages such as simple fabrication, low-cost and environment friendly. Even though the multiple advantages of the DSSCs, the efficiency of the DSSCs still limited due to the complexity of the device. That's why DSSC technology is considered to be a preferable research field in which many studies are being conducted to increase the efficiency of the device.

The objectives of this thesis are to prepare dye sensitized solar cells (DSSCs) using titanium dioxide (TiO_2) as a semiconducting layer based on eosin Y dye with adding some modifications to the structure of the device. These modifications include changing the dyeing duration of TiO_2 films, preparing a derivative of eosin Y solution acting as a new photosensitizer, changing the pH of the dye solution and adding ZnO blocking layers.

The results showed that dyeing the TiO_2 films for 3 hours can lead to a better performance of the assembled DSSC. In addition, a derivative of eosin Y was prepared by adding phenylhydrazine hydrochloride solution to the eosin Y solution in a molar ration 1:1 which contributed in enhancing the efficiency of the assembled DSSC.

The treatment of the dye solutions with phosphoric acid resulted in better performance in comparison with hydrochloric acid and nitric acid treatment.

The mechanism used in suppressing the recombination of injected electrons with both the redox electrolyte and the oxidized dye is adding ZnO blocking upper-layers which act as a barrier. By adding the ZnO upper layers, the performance of the DSSC was improved.

الملخص

تُعتبر الخلايا الشمسية الصبغية تكنولوجيا جديدة و تُصنَّف بأنها الجيل الثالث في تكنولوجيا الخلايا الشمسية. للخلايا الشمسية الصبغية مزايا عِدَّة منها بساطة تصنيعها، وتكلفتها المنخفضة، كما أنها تُعتبر صديقة للبيئة. ولكن على الرغم من هذه المزايا إلّا أنَّ كفاءة الخلايا الشمسية الصبغية لاتزال محدودة، وذلك بسبب تعقيد بناء هذه الخلايا. هذا السبب قد جعل البحث في الخلايا الشمسية الصبغية مجالاً خصباً ومفضلاً حيث تُبذل فيه الكثير من الدراسات والتي تسعى جميعها لزيادة كفاءة الخلايا الشمسية الصبغية.

إن أهداف هذا البحث هي تصنيع خلايا شمسية صبغية باستخدام ثاني أكسيد التيتانيوم (TiO_2) كطبقة شبه موصلة معتمدةً على صبغة إيوسين (Y)، مع إضافة بعض التحسينات إلى بُنية هذه الخلايا. هذه التحسينات تشمل تغيير مدة صبغ أفلام (TiO_2)، وتحضير صبغة مُشتقة من محلول صبغة الإيوسين (Y) والتي تعمل كمحفِّز ضوئي جديد، إلى جانب تغيير درجة حامضية (pH) محلول الصبغة المُستخدم، و إضافة طبقات من أكسيد الزنك (ZnO) والتي تعمل كطبقة عازلة في الخلايا الشمسية الصبغية.

وتظهر النتائج أنَّ صبغ أفلام (TiO_2) لمدة ثلاث ساعات يساهم في تحسين أداء الخلايا الشمسية الصبغية، كما أنَّ الصبغة المُشتقة من إيوسين (Y) والتي تمَّ تحضيرها من خلال إضافة محلول هيدروكلوريك فينيل هيدرازين إلى محلول الإيوسين (Y) بنسبة مولية 1:1 قد أدى إلى زيادة كفاءة الخلايا الشمسية الصبغية.

بالإضافة إلى ما سبق، فإنَّ معالجة محاليل الصبغة بحمض الفوسفوريك قد أعطى أداء افضل في الخلايا الشمسية الصبغية مقارنة بمعالجة محلول الصبغة بكلٍ من حمض الهيدروكلوريك وحمض النيتريك.

إنَّ الآلية المتَّبعة لمنع إعادة ارتباط الإلكترونات مع كلٍّ من سائل الالكتروليت و الصبغة المتأكسدة هي إضافة طبقات عازلة عُليا من أكسيد الزنك (ZnO) والتي تعمل كحاجز. حيث تحسن أداء الخلايا الشمسية الصبغية بشكل جيد عند إضافة تلك الطبقات العليا من أكسيد الزنك.

Dedication

To my family

With Love and Respect

Acknowledgment

In the Name of Allah. I acknowledge my thanks to the greatest Allah, for His bless and guidance.

I would like to express my sincere thanks and gratitude to my supervisors Dr. Sofyan Taya and Dr. Taher El-Agez. Despite being busy in various activities, they were always available for their excellent guidance.

I also thank the staff members in Physics department at IUG for their continued support, a special mention for the support and assistance given by Hatem El-Ghamri during experimental work.

Finally, I am grateful to every individual who has helped me during my master study.

Table of Contents

List of Tables

List of Figures

List of Abbreviations

T	Absolute temperature
A	Absorbance
ACN	Acetonitrile
AM	Air mass
GaAlAs	Aluminum gallium arsenide
a-Si	Amorphous silicon
ARF	Anti-reflecting film
a.u.	Arbitrary unit
k_B	Boltzmann constant
Cd-Te	Cadmium Telluride
COOH	Carboxylic group
N3	Cis-Bis(isothiocyanato) bis(2,2'-bipyridyl-4,4'-dicarboxylato ruthenium(II)
Co	Cobalt
c	Concentration
E_{CB}	Conduction band
CIGS	Copper-Indium-Gallium-Diselenide
CE	Counter electrode
J–V	Current density-Voltage
I_D	Current flowing through a diode
I_L	Current induced by light
I-V	Current-Voltage
D	Diffusion coefficient
I_0	Diode saturation current
DC	Direct current
N719	Di-tetrabutylammonium cis-bis(isothiocyanato)bis(2,2'-bipyridyl-4,4'-dicarboxylato)ruthenium(II)
DSSCs	Dye sensitized solar cells
E_{redox}	Electrochemical potential
eV	Electron volt
q	Elementary charge
$C_{20}H_8Br_4O_5$	Eosin-Y
S^*	Excited energy state of the dye
FF	Fill factor
$F:SnO_2$	Fluorine-doped tin oxide
FTO	Fluorine-doped tin oxide
GaAs	Gallium arsenide
GaInAsP	Gallium indium arsenide phosphide
Au	Gold

S	Ground state of the dye
HOMO	Highest occupied molecular orbital
HCl	Hydrochloric acid
3a–c	Iminocoumarin dye
2a–c	Iminocoumarin dyes
IPCE	Incident photon to current efficiency
P$_{in}$	Incident power
InSb	Indium antimonide
InAs	Indium arsenide
InP	Indium phosphide
In:SnO$_2$	Indium-doped tin oxide
ITO	Indium-doped tin oxide
I$^-$	Iodide
I$_2$	Iodine
IUG	Islamic University of Gaza
$^\circ$K	Kelvin
LHE	Light harvesting efficiency
l	Light path
LiI	Lithium iodide
R$_L$	Load resistance
LUMO	Lowest unoccupied molecular orbital
J$_m$	Maximum current density
P$_m$	Maximum power
V$_m$	Maximum voltage
MW	Mega watt
μM	Micro molar
ms	Micro second
μm	Micro-meter
mM	Mille-molar
ml	Milliliter
nm	Nano-meter
HNO$_3$	Nitric acid
NHE	Normal hydrogen electrode
V$_{OC}$	Open-circuit voltage
OCVD	Open-circuit voltage decay
S$^+$	Oxidized state of the dye
C$_6$H$_5$NHNH$_2$·HCl	Phenylhydrazine hydrochloride
H$_2$PO$_3$	Phosphonic group
H$_3$PO$_4$	Phosphoric acid
V$_{photo}$	Photo-voltage
Pt	Platinum
PEDOT	Poly (3,4-ethylenedioxythiophene)

e	Positive elementary charge
P-N	Positive-Negative
pH	Potential of hydrogen
P	Power
$\mathbf{E^{*}_{F,n}}$	Quasi-Fermi level
$\mathbf{r_s}$	Series resistance
$\mathbf{I_{SC}}$	Short-circuit Current
$\mathbf{J_{sc}}$	Short-circuit current density
$\mathbf{I_{sh}}$	Shunt current
$\mathbf{r_{sh}}$	Shunt resistance
Si	Silicon
Ag	Silver
NaOH	Sodium hydroxide
TW	Tera watt
$\mathbf{SnO_2}$	Tin dioxide
$\mathbf{TiO_2}$	Titanium dioxide
$\mathbf{TiCl_4}$	Titanium tetrachloride
T	Transmittance
TCO	Transparent conducting oxide
$\mathbf{I_3^{-}}$	Tri-iodide
UV-Vis	Ultra Violet-Visible
WE	Working electrode
$\mathbf{Zn(NO_3)_2.6H_2O}$	Zinc nitrate hexahydrate
ZnO	Zinc oxide

List of Symbols

η_{cc}	Charge collection efficiency
η_{reg}	Dye regeneration efficiency
τ_n	Electron lifetime
ϵ	Molar absorption coefficient
H	Power conversion efficiency
Φ_{inj}	Quantum yield of charge injection
τ_{rec}	Recombination time coefficient
θ	Theta
λ	Wavelength

Chapter 1
Introduction

Chapter 1

Introduction

In this chapter, an introduction to solar cells is presented beginning with a description of the energy resources and solar radiation as a main resource of energy. The next part describes the operating principles of the standard solar cells. A short discussion about the current solar cell technologies is given and as a related issue, the advantages and the drawbacks of solar cells are presented in this chapter. This chapter also gives a general idea about the electricity crisis in Gaza Strip.

1.1   Energy resources

Energy on our planet can be divided into two main categories: renewable and non-renewable energy. Fossil fuels such as petroleum, coal and natural gas are the main non-renewable energy resources (Chen, 2011). For a long time, the use of these resources has caused many problems such as air pollution, water pollution and climate change (Jacobson & Delucchi, 2011). For an optimal industrial development, only renewable energy can be considered a good option as a cheap and a clean energy source (Chen, 2011). Water, wind, wave, tide, geothermal and solar energy are the most familiar types of the renewable energy. Direct solar energy is the main source of the renewable energy and any other renewable energy source can't exist without it (Jäger et al., 2014). Today, the renewable energy contributes with 27.7% to the total energy production in the world (Adib, 2015).

1.2   Solar energy and solar radiation spectrum

Solar energy is available at all locations on the earth and classified as the most promising renewable energy sources for the energy needs. The earth receives 1.4×10^5 TW per year from it and about 3.6×10^4 TW of this power is usable (Hosenuzzaman et al., 2015). The theoretical sun spectrum is so close to the black-body spectrum at a temperature of $5800 ^\circ K$, but due to the presence of air, the solar radiation is continuously attenuated by the absorption by different gases in atmosphere such as: H_2O, CO_2 and O_3 (Kuzmych, 2014). As a result, the practical

sun spectrum can vary from this theoretical one, depending on the path that the solar radiation is passing through. Therefore, the distance of the sunlight path through the atmosphere is a very important parameter in describing the solar spectrum. This parameter is characterized by the optical air mass which is defined as the ratio of the path length of sunlight when the sun is at an angle θ to the path length of sunlight when the sun is at the zenith itself (Zeman, 2003).
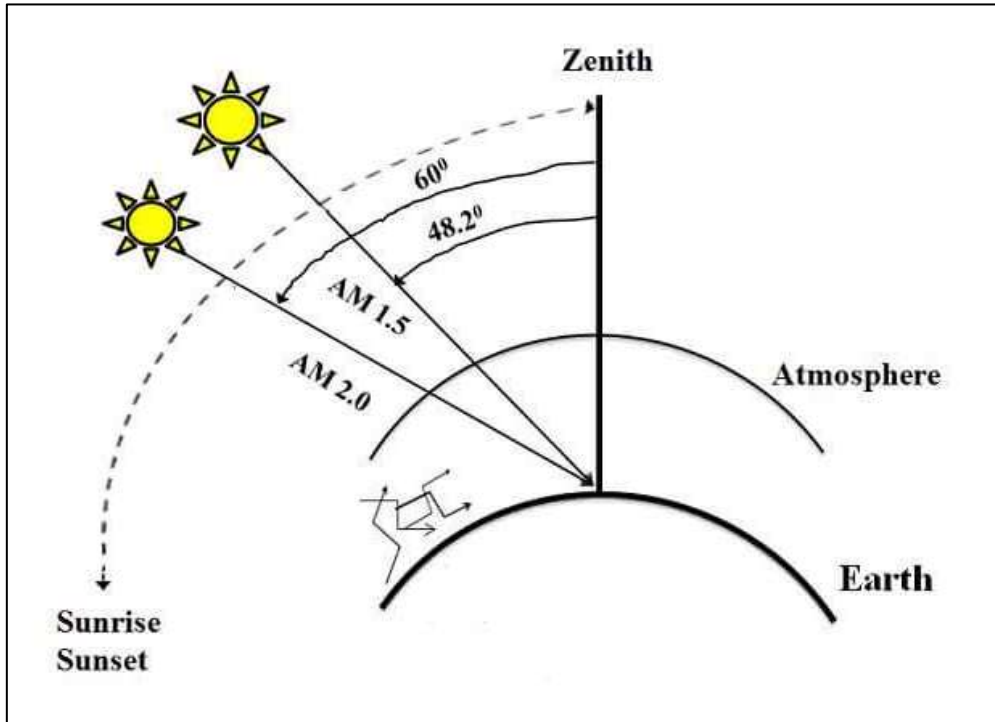
Figure (1.1): Diagram for air mass.

$$Air\ mass = (\cos \theta)^{-1} \tag{1.1}$$

where θ is the angle of the sun postion to the zenith. From this equation many solar spectra can be measured. For example, when the sun is at the zenith, the optical air mass equals one and the spectrum is described by air mass one (AM1). When the sun is at 60° from the zenith, the optical air mass equals two and the spectrum is described by air mass two (AM2). For solar radiation studies and measurements, the air mass 1.5 has been chosen as a calibration standrad which corresponds to 48.2° from the sun's position to the zenith and is related to 1000 W/m^2 (Zeman, 2003).

3
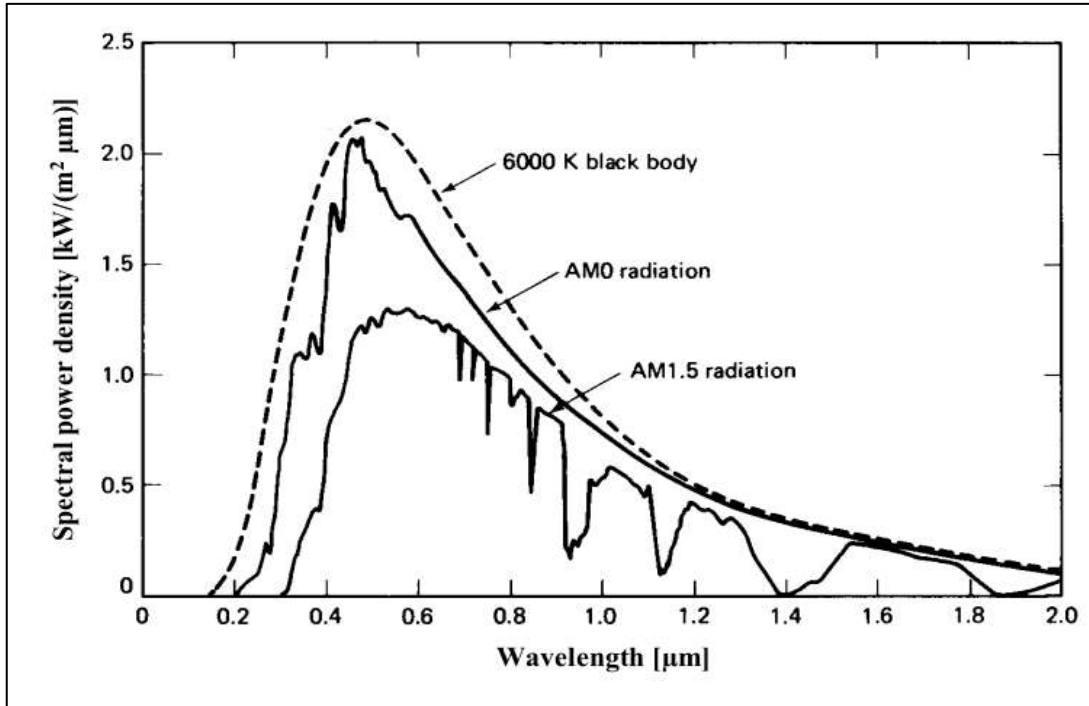
Figure (1.2): Spectral power density of sunlight for different solar spectra.

1.3   Operating principles of the standard solar cells

Solar cell consists of a p-doped semiconductor and an n-doped semiconductor placed in contact to form a P-N junction. When no external bias is applied, electrons in the n-type side tend to flow towards the p-type side and the holes in the p-type side tend to flow towards the n-type side. This diffusion of electrons and holes resulting in the creation of minority positively charged ions in the n-type side and negatively charged minority ions in the p-type side. As a result, a space-charge region or a depletion region is created at the p-n junction, and an electric field is set up through the depletion region, as shown in figure (1.3). This electric field is referred as the built-in potential which opposes the normal diffusion of electrons and holes through the junction (Aribisala, 2013).

The solar cell can operate properly when the positive terminal of the load is connected to the p-type side of the solar cell and the negative terminal of the load is connected to the n- type side of the solar cell, as shown in figure (1.4), (Khan, 2013). Under illumination, the light absorption generates electron-hole pairs at the depletion region, which can be separated by the built-in electric field and a photo current is

4

produced through the circuit, which is like a forward biased diode with a photo-voltage (Halme, 2002).
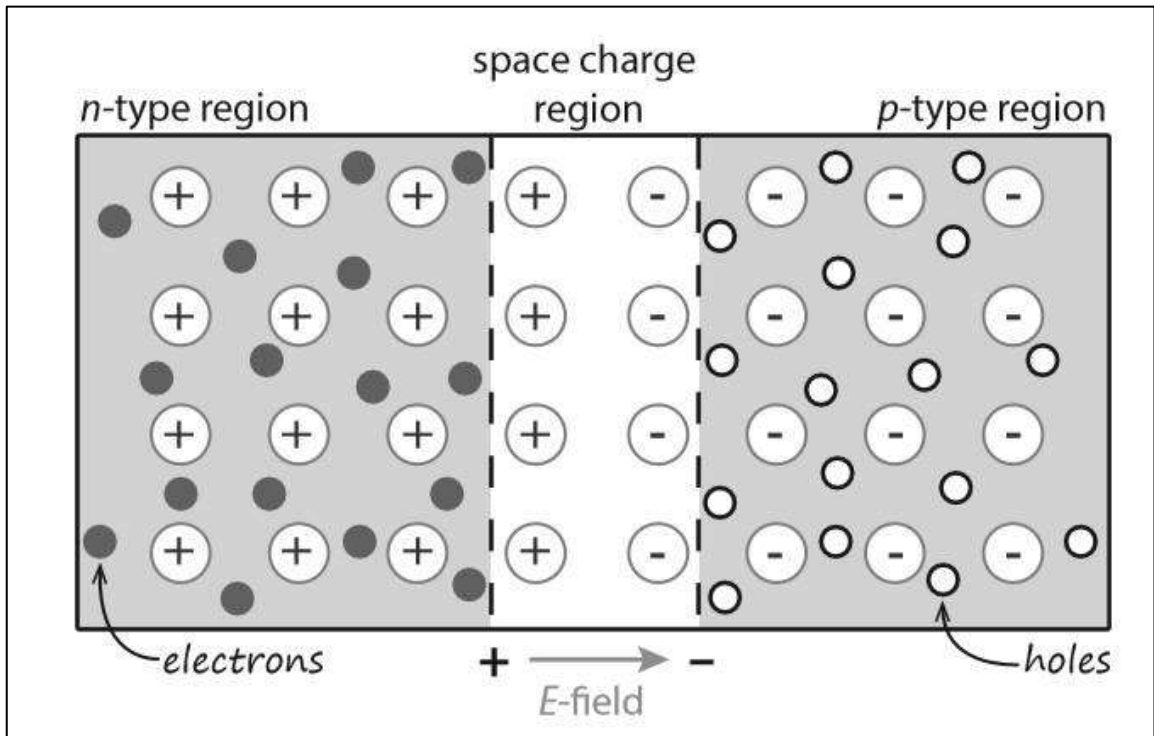
Figure (1.3): Formation of space charge region in a P-N junction under unbiased condition.
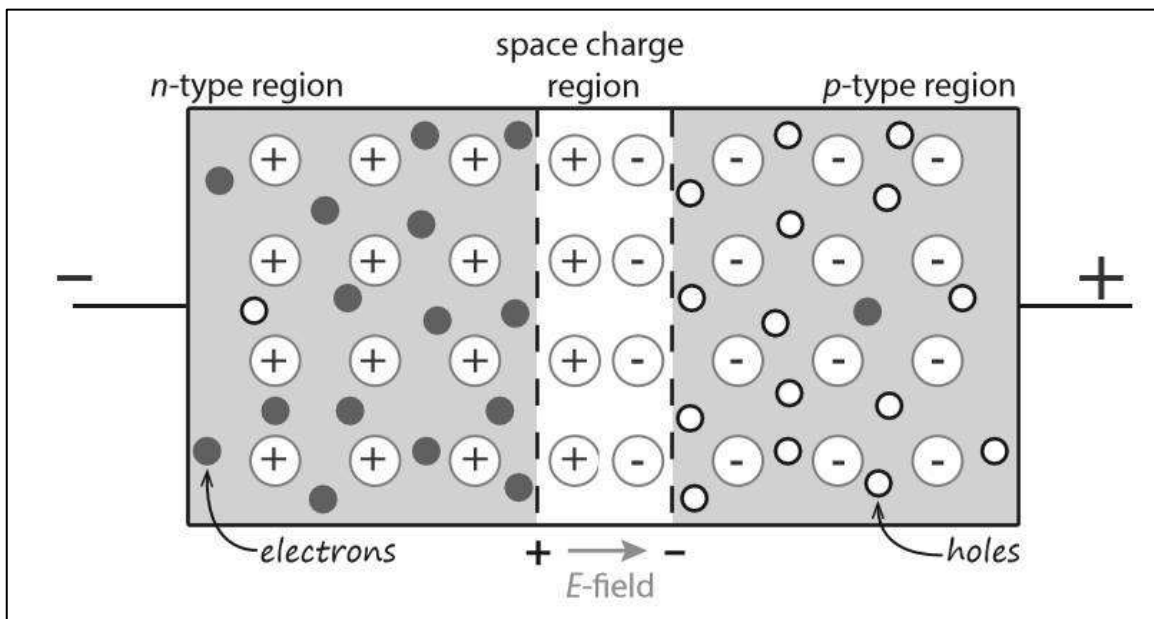
Figure (1.4): P-N junction under forward biased condition.

The operation of converting sunlight into electrical current in the solar cell is divided into three main steps:

1. Light absorption.

2. Charge separation.

3. Charge collection.

The detailed processes that occur in each step can vary between different types of solar cells (Halme, 2002). Generally, the design and performance of a solar cell depend on the following parameters:

1. Dopant concentrations: dopants can be donor atoms which donate free electrons producing n-type material or acceptor atoms which receive electrons producing p-type material. The width of the depletion region is determined by the dopant concentrations (Zeman, 2003).

2. Mobility: mobility is a main factor in determining electrons and holes transport due to the drift through the solar cell, where the drift is the motion of charged-particles in presence of an electric field (Zeman, 2003).

3. Diffusion coefficient: which is a main factor in determining electrons and holes transport due to diffusion, where the diffusion is the motion of the charge carriers from high carriers concentrated region into low carriers concentrated region (Zeman, 2003).

4. Lifetime: which is a central parameter in recombination-generation process that occurs in the solar cell, lifetime is the average time that an excess minority carrier can survive before being annihilated (Zeman, 2003).

5. Diffusion length: it's another central parameter in the recombination-generation process and is defined as the average distance that the minority carriers can diffuse through the solar cell before being annihilated (Zeman, 2003).

6. Band-gap energy, absorption coefficient and refractive index, all these factors can determine the efficiency of the solar cell in absorbing visible radiation (Zeman, 2003).

1.4   Current solar cell technologies

1.4.1   Crystalline and multi-crystalline silicon solar cells

Solar cells based on crystalline and multi-crystalline silicon are simply solid state semiconductor p-n junction devices converting sunlight into current by the photovoltaic effect principle (Green, 1982). The crystalline silicon solar cell is known as the first generation photovoltaic technology, where the theoretical efficiency of this type is up to 25% and it's about 20.4% in multi-crystalline silicon solar cells (Green et al., 2010). It is considered the most produced in the world which estimated to 80% in the solar cell market.

The first crystalline silicon solar cells were produced in the late 1950s to provide electrical power for satellites (Aribisala, 2013). This industry has been widely developed to cover manny fields such as telecommunication equipments, weather monitoring systems, military purposes and solar power system (Aribisala, 2013). This type of solar cells is considered the most expensive, since it requires high purity silicon and that purification process is expensive and slow to grow (Hegedus & Luque, 2003).

1.4.2   Inorganic thin film solar cells

Thin-film solar cells are referred to be the second generation photovoltaic technology, which aims to reduce the expensive production cost of wafers in silicon solar cells by using a few microns thick layers of semiconductors, that are usually deposited onto a supporting low-cost substrates such as glass or flexible plastic. This active semiconductor layer can absorb significant amounts of light because of the strong absorbance in the materials and electrons have to travel a very short distance through the thin films ((Hegedus & Luque, 2003).

The most common materials used in the inorganic thin film solar cells are as follow:

a- **Amorphous silicon (a-Si):** amorphous silicon was employed in the beginning of thin film solar cells. This type is commonly used in devices that

require little power because of low efficiency rates, which is about 10.1% (Gree et al., 2010).

b- **Thin film crystalline silicon:** this technology uses a layer of crystalline silicon with flat surface which is deposited on a surface of a reflector, leading to a light trapping thruogh the solar cell, which in turn reduces the silicon quantity used in the solar cell. A Layer of 5-50 mm thickness can be achieved by this technology (Halme, 2002) and the efficiency is about 12.2% (Goetzberger & Hebling, 2000). A supporting layer must be added under the thin film crystalline silicon such as a low-grade silicon or any other materials like graphite or glass (Halme, 2002).

c- **Cadmium Telluride (Cd-Te)** : Thin film solar cells based on Cd-Te is about 16.5% efficient which is better than the amorphous silicon in both power efficiency and manufacturing costs. Despite these benefits of Cd-Te solar cells, there are some drawbacks. For example, the disposal and recycling are both dangerous and costly, because cadmium is a heavy metal and considered a carcinogen, which can accumulate in living tissues.

d- **Copper-Indium-Gallium-Diselenide (CIGS):** Thin film solar cells based on CIGS is about 19.4% efficient, which is the highest effeciency among the previous thin film solar cells (Green et al., 2010). The limited amount of indium makes it an expensive technology (Green, 2007).

1.4.3   III-V Semiconductors

This type of thin film solar cells are composed of elements from the third and the fifth groups such as Gallium arsenide (GaAs), Gallium aluminum arsenide (GaAlAs), Gallium indium arsenide phosphide (GaInAsP), Indium arsenide (InAs), Indium antimonide (InSb) and Indium phosphide (InP). These compounds have small band gaps and high absorption, making them suitable for photovoltaic devices (Halme, 2002). Efficiency of about 40% has been achieved by III-V semiconductor compounds, but these materials are extremely expensive (Tanabe, 2009).

1.4.4   Dye-sensitized solar cells

Dye-sensitized solar cells (DSSCs) are a special kind of solar cells based on nano-crystalline metal oxide electrodes and an organic dye. They convert visible light into electrical current when the organic dye absorbs light which in turn mimics the process of photosynthesis. DSSCs have a promising future in photovoltaic applications and have been studied worldwide.

DSSCs are a new attractive technology because they can be more cheap, portable, light weight and flexible relative to classical solid state solar cells (Grätzel, 2001), where the efficiency of DSSCs has reached about 11% (Green et al., 2010).

The previous solar cell technololgies are presented in figure (1.5).
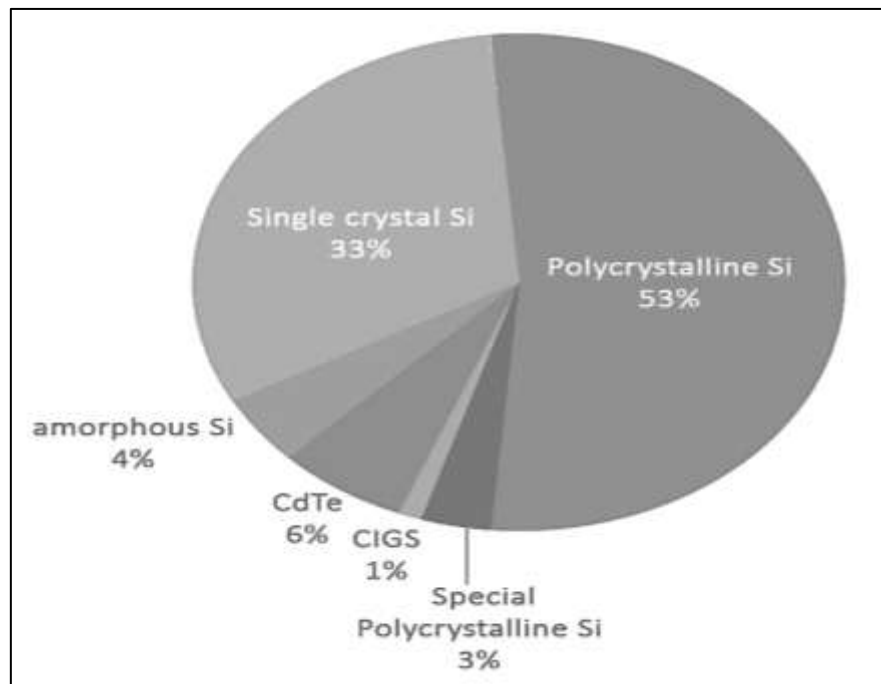
Figure (1.5): Production of PV technologies in 2015 (Hosenuzzaman et al., 2015).

1.5   Advantages and drawbacks of solar cells

Solar cells can be considered an environmentally friendly with neither noise nor emissions produced from them. Moreover, solar cells don't require fuel or water

to run, where the electric current can be generated when the light exists. In addition they can be operated in the cloudy weather conditions.

Although all of these advantages, solar cells still have some drawbacks. For example, solar cells can't operate without light and they require a large area to be installed if a high power is needed. Moreover, solar cells generate a direct current (DC current), so it's suitable for the DC appliances or an inverter must be used in off-grid. Finally, the energy produced by the solar cells need to be stored in an energy storage system such as batteries (Zeman, 2003).

1.6 Electricity crisis in Gaza Strip

Gaza Strip has been suffering from a lack in electricity supplies, where the demand of electricity is about 450 MW, while the available supplies are only about 230 MW provided from three major sources, the first source is the electricity company with 120 MW supply, the second source is the power station in Gaza with average production of 80 MW and the third source is the Egyptian electricity grid with 27 MW supply (Radwan, 2015). This means that the disability of electricity need is about 50% in Gaza Strip, especially that Gaza Strip is considerd a high densely populated area with a population of about 3823 persons/km^2. These things mak the electricity need a real crisis affecting many fields in the everyday life in Gaza Strip. Solar energy can serve in solving electricity lack in Gaza Strip, where the geographical location of Gaza Strip makes it one of the most relatively sunny regions in the world with more than 300 sunny days a year and about 8 hours brightness a day. This means that Gaza Strip receives a solar irradiance of about 2000 kWh/m^2 annually (Jasser, 2010).

Recently, residents in Gaza Strip began using silicon solar cells in the form of big solar panels installed on rooftops to generate electrical energy, to overcome the energy crisis. However, the current reliance on solar power in Gaza Strip doesn't exceed the 5% because of the high costs of solar panels (Jasser, 2010).

Chapter 2
Dye Sensitized Solar Cells

Chapter 2
Dye Sensitized Solar Cells

In this chapter, an overview of dye sensitized solar cells (DSSCs) is presented. The components of DSSC with a full description of related conditions to each component are also provided in section 2.2. The operational principles of DSSCs are presented in section 2.3. After that, the main parameters of DSSCs are discussed and the equivalent circuit of the DSSC is analyzed.

2.1   Introduction

Dye sensitized solar cell (DSSC) is a new technology developed by O'Regan and Grätzel, in which they used a ruthenium based dye with an active layer made from titania (TiO_2) (O'Regan & Grätzel, 1991). It is widely accepted that DSSCs are a promising route toward simple fabrication, low-cost, environment friendly power generation, as a clean photoelectric conversion system and potential alternative to the traditional photovoltaic devices (Hagfeldt & Graetzel, 1995). In its simplest structure, as shown in figure (2.1), a DSSC consists of the following components: a transparent conducting oxide (TCO) substrate which acts as the anode, a nano-crystalline TiO_2 semiconductor film, an organic dye acts as a photo sensitizer, an electrolyte solution containing iodide (I^-)/ tri-iodide (I_3^-) redox couple and a platinized counter electrode acts as the cathode (Ramasamy et al., 2013).
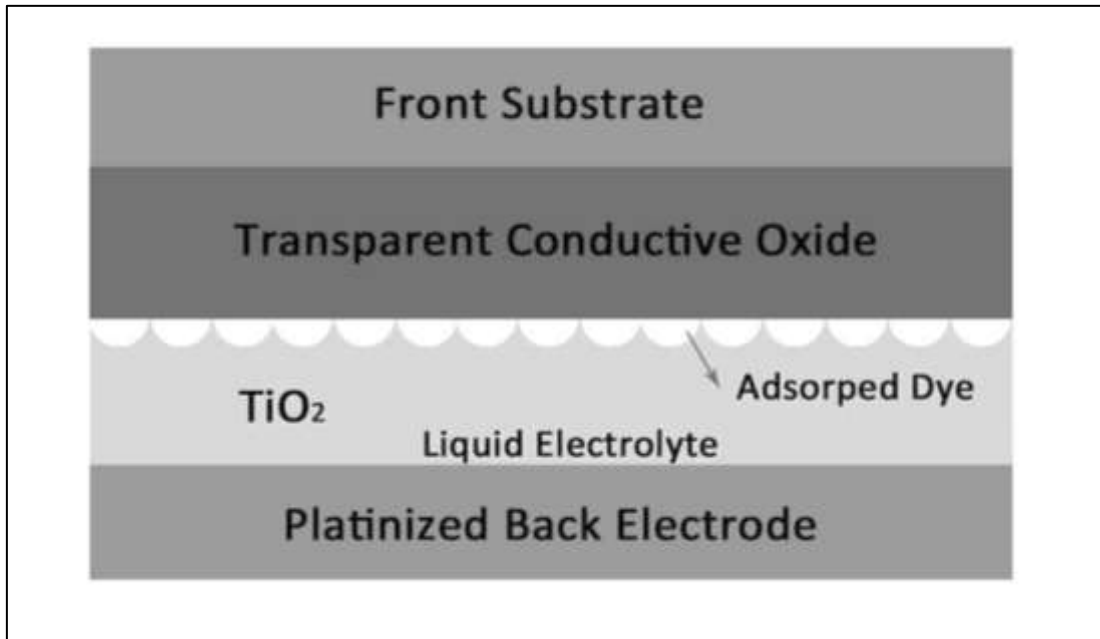
Figure (2.1): Basic structure of DSSC.

2.2   Basic components of DSSC

2.2.1   Transparent conducting substrates

The structure of the DSSC includes two transparent glass substrates treated with a transparent conductive oxide layer which is usually abbreviated as TCO layer. Indium-doped tin oxide (In:SnO$_2$, ITO) and fluorine doped tin oxide (F:SnO$_2$, FTO) are the most common conducting oxides used in DSSCs. The front TCO layer is the anode of the cell and the back TCO layer is the cathode. Both TCO layers function as a current collector in the DSSC (Gong et al., 2012).

Two important features have to be considered in TCO substrates: the high transparency of the TCO front layer allowing the sunlight to pass through the DSSC without absorption and the high photo-reflection of the back TCO layer in order to reflect back the transmitted light into the dye. The second feature of the TCO substrates is the low electrical resistivity that allows the electrons to pass through the substrates with a minimal loss apart from high temperatures (Gong et al., 2012). For example: indium tin oxide (ITO) is over than 80% transparent and the sheet resistance is about 15Ω/□ while fluorine tin oxide (FTO) has 70–80% transmittance and the sheet resistance of FTO is less than 12Ω/□ (Yang, 2008).

The effect of high temperature on the sheet resistance of ITO and FTO appears clearly in the sintering stage, since fabrication process of DSSCs requires sintering TiO_2 paste on TCO substrates at high temperature (450-500)℃ to improve the electronic contact (O'Regan & Grätzel, 1991). The ITO films in that stage are exposed to high temperature and the sheet resistance increases drastically which affects the cell efficiency, whereas the sheet resistance of FTO films remains unchanged after the thermal treatment. This means that FTO is more preferred than ITO in DSSCs due to the thermal stability of FTO (Sim et al., 2010).

2.2.2 TiO_2 semiconductor as a photo-electrode

An n-type semiconductor in the form of wide band gap metal oxides such as TiO_2, ZnO and SnO_2 are used as a deposited layer on a transparent conducting oxide (TCO) substrate in the DSSC (Kuzmych, 2014). The wide band gap of the semiconductors, as shown in figure (2.2), prevents any generating of charge in the metal oxide itself when it is exposed to visible light, ensuring the main task of the wide band gap semiconductors, which is the carrier transport in the DSSC (Gong et al., 2012).

The most efficient metal oxide used in the DSSCs is the titanium dioxide (TiO_2) in its porous nano-crystalline form which was firstly employed by Grätzel and his co-workers. This structure of TiO_2 increases the internal surface area of the electrode allowing a large amount of dye to be adsorbed on the electrode (Zeman, 2003). Typical TiO_2 films used in the DSSCs have a thickness of around 10 μm and the size of its nano-particles is in the range of (10-30) nm in diameter (Kuzmych, 2014).

TiO_2 has three natural forms: rutile, anatase and brookite. The most stable form is rutile, since it's considered to be temperature-independent but for the DSSCs performance, the anatase form is more active than rutile because the band gap of anatase is about 3.2 eV which is larger than rutile's band gap of about 3eV (Sao et al., 2010).

Nowadays, the most common TiO_2 product is DeGussa P25 which has 80% anatase and 20% rutile in which the diameter of the particle is 25 nm (Gong et al., 2012). TiO_2 has many advantages such as its high photosensitivity, structural stability under solar irradiation, low cost and its non-toxicity. All these features makes TiO_2 a preferable material used in DSSCs.
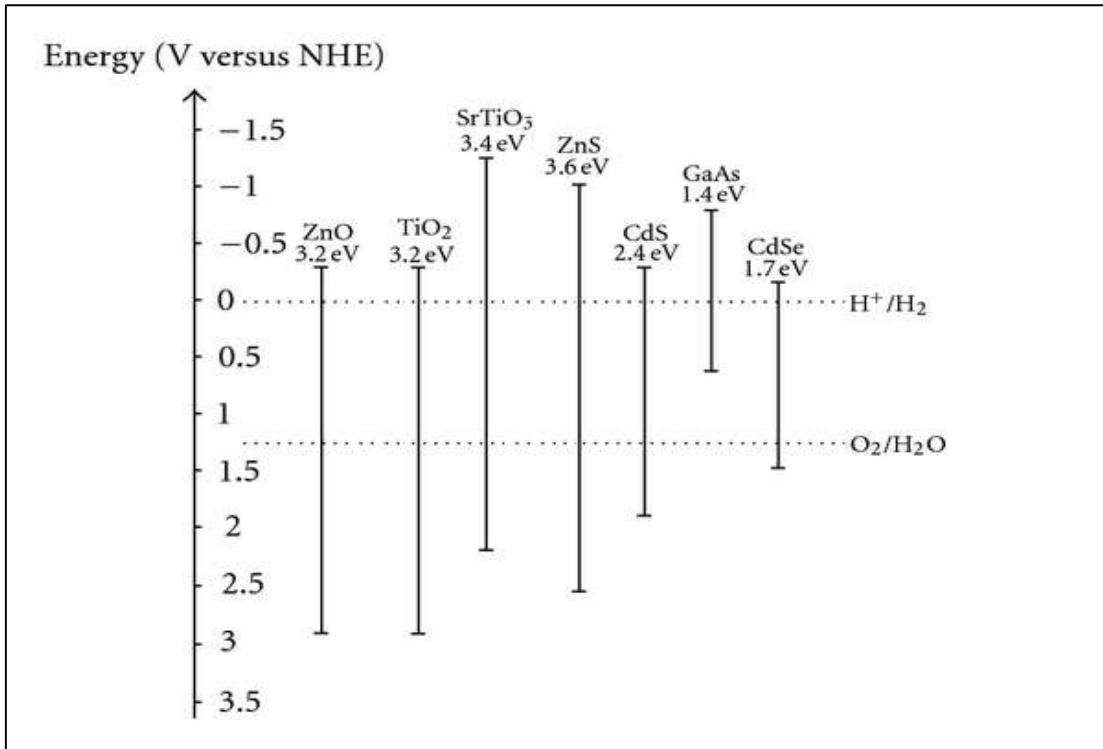
Figure (2.2): Band positions of several semiconductors

2.2.3 Dye as a photosensitizer

In DSSC, the surface of the porous TiO_2 electrode is usually coated with an organic dye molecules that absorb the incident light. The dye injects the excited electrons into the wide band gap TiO_2 and become regenerated by the electrolyte.

2.2.3.1 Main structure of organic dyes

As illustrated in figure (2.3), an organic dye consists of a hydrophobic electron donor, connected via π bridge unit to a hydrophilic electron acceptor, where the electron acceptor of the dye acts as the anchoring site on the TiO_2 photo anode (Obotowo et al., 2016).

Adsorption of the dye molecules to TiO₂ surface takes place via the anchoring groups located at the end of the dye molecules, where a chemical bond is formed between the anchoring group and the TiO_2 surface by donating a proton to the TiO_2 lattic (Halme, 2002). The most common anchoring groups attached to the dye molecules are the carboxylic group (COOH) and phosphonic group (H_2PO_3).

Moreover, the position of the energy levels in the dye is a main point in its structure, the two energy states that have a great importance are: the ground state which is referred to the highest occupied molecular orbital (HOMO) and the excited state or the lowest unoccupied molecular orbital (LUMO). Between these two energy states, there is a small gap enables a large harvesting of low energy photons that gives a high photocurrent of the cell (karlsson, 2011).
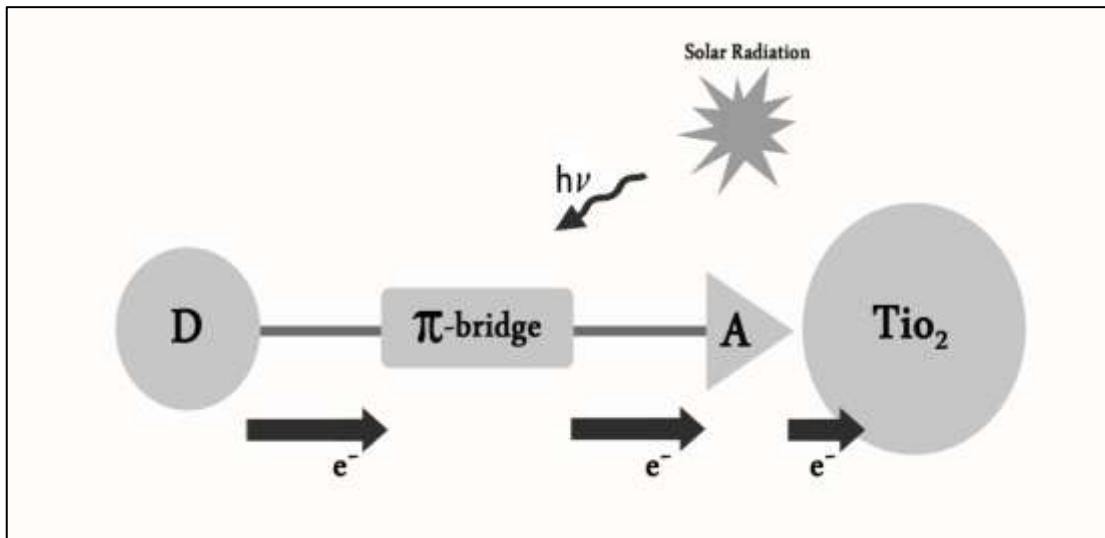
Figure (2.3): Donor-π bridge- acceptor organic dye and their electrons transfer under illumination.

2.2.3.2 Main conditions to be considered in choosing the photo-sensitizer

In order to get high sensitization of the dye, there are some conditions have to be fulfilled in the chosen dye, which are as follow:

1- The dye should have a broad absorption spectrum covering the whole visible region and some of the near infra-red region (Karlsson, 2011)
2- The highest occupied molecular orbital (HOMO) should be localized around the donor group in the dye itself and should lie below the energy level of the

16

electrolyte since the oxidized dye have to be regenerated by the electrolyte (Obotowo et al., 2016).

3- The lowest unoccupied molecular orbital (LUMO) should be localized around the anchoring group in the dye itself and should lie above the conduction band of the TiO_2 to facilitate a quick electron injection into TiO_2 lattice.

4- A high extinction coefficient of the dye that enables the use of thinner TiO_2 films with a high degree of light absorbtion (Karlsson, 2011).

5- The donor part of the organic dye have to be hydrophobic, to prevent any contact between the electrolyte and the anode and to prevent any possible desorption of the dye in water or in the electrolyte redox (Obotowo et al., 2016). The dye has not to be aggregated on the TiO_2 surface in order to avoid non-radiative decay of the excited state to the ground state.

6- The dye should have high solubility in the solvent which can be water or alcohol to ensure a complete adsorption of the dye on TiO_2 surface.

7- Low toxicity of the dye and possibility to be recycled.

8- The dye should have thermal and chemical stability when the device is under illumination.

2.2.3.3 Common dyes as sensitizers

The most efficient DSSCs are based on ruthenium bipyridyl organometallic complexes such as the N3 dye, N719 dye and the black dye. Generally, ruthenium dyes have absorbance range from visible to near-infrared wavelengths. Figure (2.4) shows the molecular structures of these three dyes (Rayan, 2009).
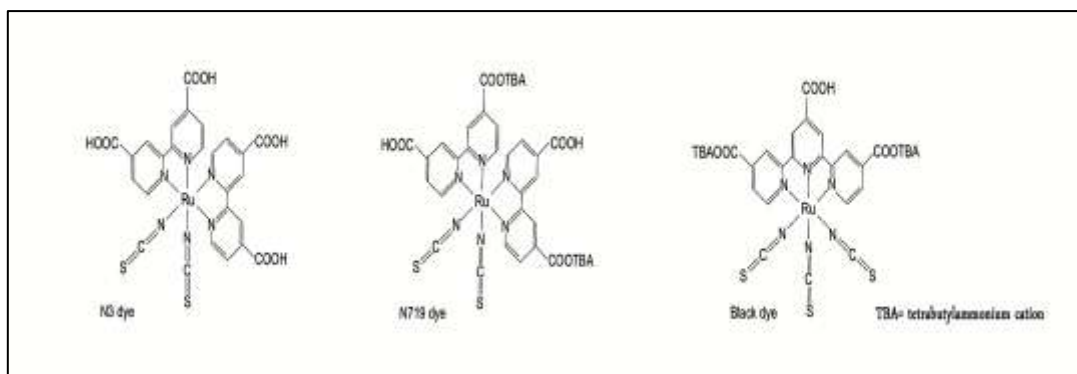
Figure (2.4): The molecular structures of N3 dye, N719 dye and black dye.

2.2.4 Electrolyte

The electrolyte used in the DSSCs consists of iodine (I^-) and triiodide (I_3^-) as a redox couple dissolved in a solvent such as acetonitrile (ACN). Electrolyte is responsible for regenerating the oxidized dye.

Some conditions in the used electrolyte have to be taken into account, which are as follow:

1- Ability of the electrolyte solvent to dissolve ingredients to ensure high concentration of charge carriers (I^-/ I_3^-) in the electrolyte (Toivola, 2010).
2- Low volatility of the solvent especially when the device is exposed to solar radiation (Toivola, 2010).
3- High viscosity of the solvent to facilitate the diffusion of charges between the two electrodes (Toivola, 2010).
4- Absence of absorbance in the visible region to prevent any absorption of incident light by the electrolyte (Halme, 2002).
5- High stability of the reduced part (I^-_3) and oxidized part (I^-) of the redox couple to ensure a long operating life (Halme, 2002).
6- High diffusion coefficient of the solvent to enable efficient mass transport (Halme, 2002)
7- The solvent should be not toxic and a low cost material.

2.2.5 Counter-electrode

The last component of the DSSC is the counter electrode, which is responsible for regenerating the redox couple (I^-/ I_3^-) by reducing the tri-iodide to iodide.

Counter electrode is prepared by depositing a thin layer of platinum onto a transparent conducting oxide (TCO) substrate, where the most used TCOs are Indium-doped tin oxide ($In:SnO_2$, ITO) and fluorine doped tin oxide ($F:SnO_2$, FTO) (Hagfeldt et al., 2010). As mentioned before, FTO is more preferred than ITO in DSSCs due to its thermal stability.

Platinum layer is added to catalyze the reaction on the counter electrode. Without a platinum layer, the counter electrode has a charge transfer resistance of about 10^6 $\Omega/\square$, while with the platinum, the resistance is about 1 $\Omega/\square$. So, the performance of counter electrode is improved by adding the platinum layer (Hagfeldt et al., 2010; Tolvanen, 2003). Since the Pt layer is almost transparent, the platinized counter electrode can serve as a mirror reflecting back the transmitted light through the cell. In addition, platinum has a high catalytic activity and a high chemical stability in the electrolyte (Toivola, 2010).

Other materials were used as catalysts on the counter electrode, among these material conducting polymers such as polyaniline and Poly (3,4-ethylenedioxythiophene) (PEDOT) and the carbon materials such as graphite and carbon black. The problem of using these materials is that a high thick layers have to be introduced to reach the required catalytic activity, these thick layers slow down the cell performance. Thus, platinum is the best catalyst can be used in the DSSC (Toivola, 2010; Hagfeldt et al., 2010).

2.3   Principles of operation in DSSCs

In DSSC, the mechanism of converting light into electrical current is achieved through four main processes, as shown in figure (2.5), which are as follow:

1- Light absorption and dye excitation.
2- Charge separation and electron injection.
3- Charge collection.
4- Dye regeneration.
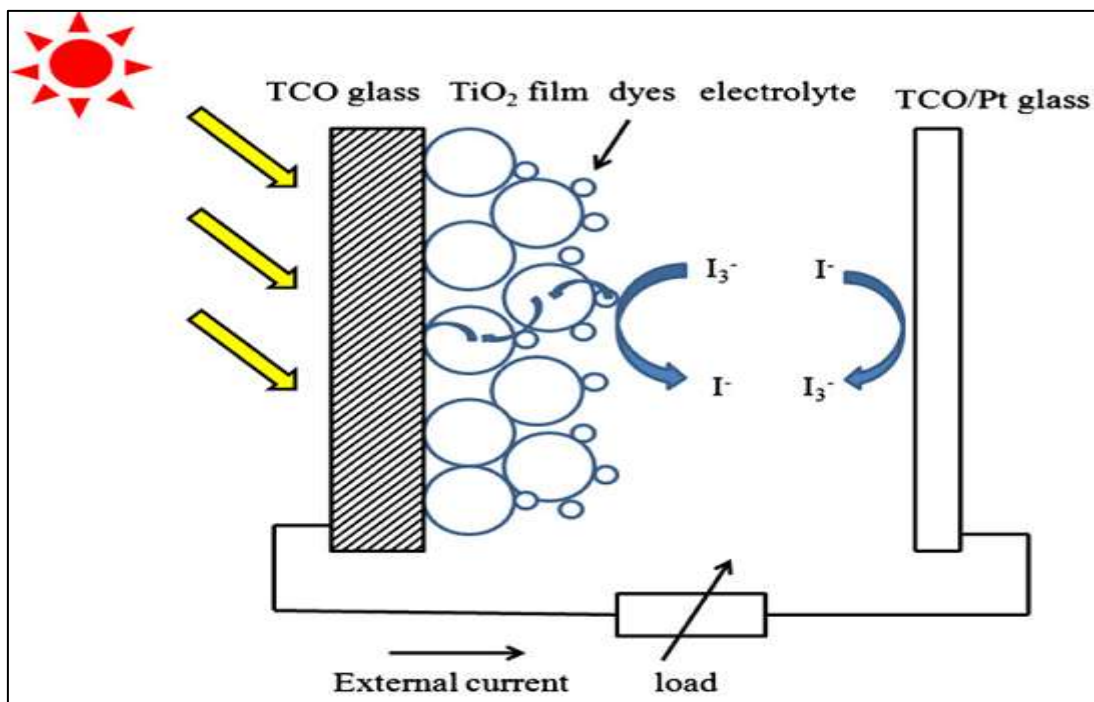
Figure (2.5): Operations in DSSC.

2.3.1 Light absorption and dye excitation

When the DSSC is under illumination, the light passes through the FTO substrate and reaches the dye molecules which are adsorbed on the TiO_2 surface. There, the light is absorbed by dye molecules when that light matches the energy difference between the highest occupied molecular orbital (HOMO) and lowest unoccupied molecular orbital (LUMO) of the dye molecules. Then, the dye molecules will be excited and one electron will be transferred from HOMO to LUMO in each molecule as shown in equation (2.1). The lifetime of the excited state (S^*) is in the order of nanoseconds. For many organic dyes, the absorption onset is in the range of 720 nm which corresponds to a photon of energy 1.72 eV (Khan, 2013).

$$S + h\upsilon \rightarrow S^* \tag{2.1}$$

2.3.2 Charge separation and electron injection

The first factor which is responsible for the charge separation is the position of energy levels in the TiO_2, the dye and the redox couple. The LUMO level of the

excited dye (S*) must be above the conduction band edge of the TiO_2, and the HOMO level have to be below the chemical potential of the redox couple, this difference of energy levels positions results in a driving force for electron and hole separation (Halme, 2002).

The second factor is the binding between the carboxylic group (COOH) of the dye and the TiO_2, where the carboxylic group donates the TiO_2 a proton making the dye negatively charged is also responsible for the charge separation (Cahen et al., 2000). Presence of driving force will cause the excited dye (S*) to inject an electron into the conduction band of TiO_2 (equation 2.2), electron injection is a very fast process which occurs in a range of tens of femtoseconds (Cahen et al., 2001)

$$S^* \rightarrow S + e^-$$
(2.2)
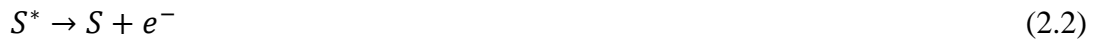
2.3.3   Charge transport and electron collection

In DSSC, charge transport includes electron transport through the nano-porous TiO_2 electrode and hole transport through the electrolyte, the two transport mechanisms occur in opposite directions as shown in figure (2.6).
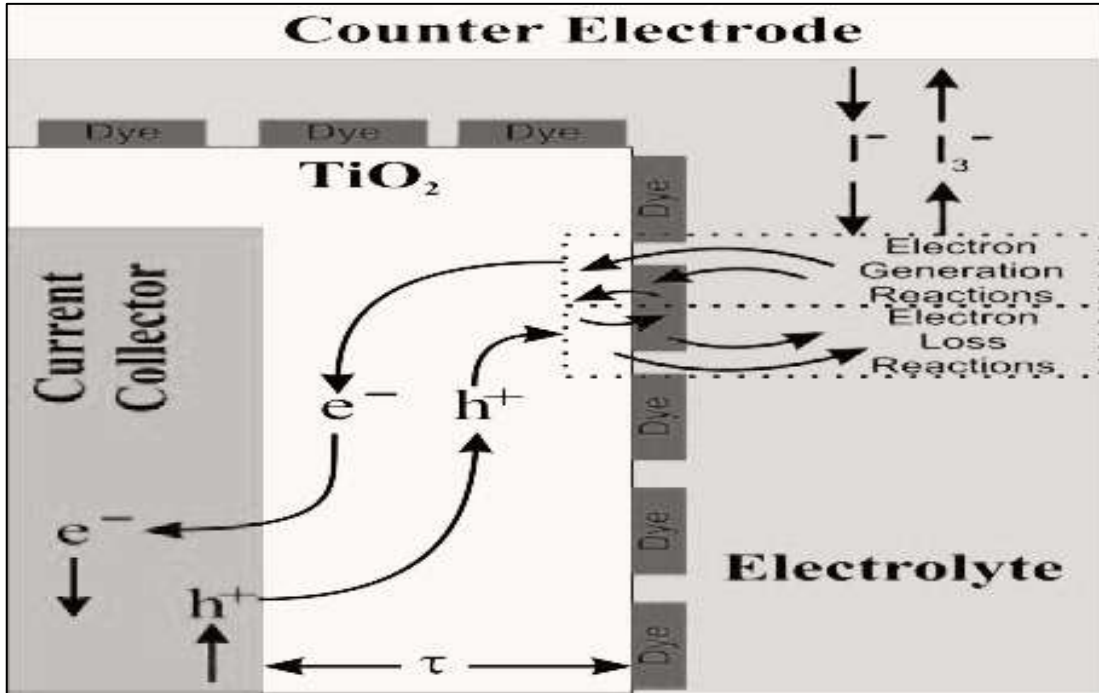
Figure (2.6): Electron and whole transport in DSSC, both mechanisms occur in opposite directions.

2.3.3.1 Electron transport and collection

The nano-porous TiO_2 consists of spherical particles with a diameter of about 25 nm. The small size of the particles prevents the formation of a space charge layer as in the p-n junction and so no electric field can exist inside the particles. Therefore, the electrons transport through the TiO_2 lattice can't be attributed to the existence of an electric field through the lattice (Halme, 2002; Khan, 2013).

The mechanism that is responsible for electron transport is diffusion through the network of individual spherical particles in the TiO_2 lattice, where the electrons jump from one particle to the next in a consequent known as trapping and de-trapping process (Hagfeldt & Grätzel, 2000). Diffusion of electrons is characterized by the diffusion length which is the average distance an electron is transported before being recombined, diffusion length can be calculated from the diffusion coefficient (D) and the recombination time coefficient (τ_{rec}) (Fredin, 2007).

$$L = \sqrt{D\,\tau_{rec}} \qquad\qquad (2.3)$$

After that, these energetic electrons are collected at the front FTO substrate and then through the external load to perform work. Finally, electrons are collected at the counter electrode.

2.3.3.2   Hole transport

The redox couple in the electrolyte acts as a hole-conducting medium, electron injection from the excited dye into the TiO$_2$ usually leaves the dye in an oxidized form (S$^+$), that oxidized dye seems to have a hole and that hole will be later filled by an electron from the iodide (I$^-$) in the electrolyte, leaving another hole in the electrolyte. This mechanism in filling holes by electrons each time makes the holes to look like moving particles (Fredin, 2007).

2.3.4   Dye regeneration

To ensure a continuous operating device, the oxidized dye (S$^+$) have to be reduced and that's can be achieved by the redox couple in the electrolyte. The oxidized dye is regenerated to its original form by oxidizing iodide (I$^-$) into triiodide (I$_3^-$), (equation 2.4). While the reduction of triiodide into iodide takes place at the platinized counter electrode using the collected electrons from the external load, (equation 2.5).

$$2S^+ + 3I^- \rightarrow 2S + I_3^- \tag{2.4}$$

$$I_3^- + 2e^- \rightarrow 3I^- \tag{2.5}$$

2.4   Losses in DSSCs

The efficiency of DSSCs is affected by losses resulting from many losses mechanisms, such as:

   I. Loss due to the relaxation of the excited dye before injecting electrons in TiO$_2$ (Zeman, 2003).

  II. Loss due to the non-absorption of long wavelengths.

 III. Loss due to the reflection of incident light.

 IV. Loss due to recombination of injected electrons with the oxidized dye.

V. Loss due to recombination of injected electrons with tri-iodide in the electrolyte (Zeman, 2003).

Since the efficiency of DSSCs is affected greatly by the last two mechanisms, they are introduced as follow

2.4.1 Recombination between the injected electrons and the oxidized dye

The recombination process between the injected electrons and the oxidized dye must be slower than the process of electron injection into the TiO_2 and also slower than the process of dye regeneration. It was reported that recombination between injected electrons and oxidized dye occurs in a range of microseconds to milliseconds, while electron injection occurs in a range of tens of femtoseconds and the dye regeneration is in a range of nanoseconds, which means that electron recombination is much slower compared to both the electron injection and the dye regeneration. In other words, the more slower electron recombination, the more efficient the cell (Tachibana et al., 1996; Kuciauskas et al., 2001).

2.4.2 Recombination between injected electrons and tri-iodide ions (dark current)

Recombination of injected electrons with tri-iodide ions (I_3^-) on the TiO_2 surface is a main loss process in DSSCs which corresponds to dark current. As shown in the following reaction:

$$I_3^- + 2e^-(TiO_2) \rightarrow 3I^-$$

(2.6)

Because of the high surface area of the TiO2, dark current usually takes place at the TiO_2/electrolyte interface. To suppress dark current, many procedures can be considered such as adding blocking layers of other semiconductor materials (Nazeeruddin et al., 1993; Huang, 1997).

2.5   Main parameters in DSSCs

2.5.1   Short-circuit current (I_{SC})

It's the current obtained from the solar cell when the electrodes of the solar cell are short circuited, i.e. when the load resistance is zero (Khan, 2013). The value of I_{sc} can vary according to many factors such as light intensity, amount of light absorbed by the dye, rate of electron injection and regeneration of the oxidized dye (Karlsson, 2011).

To adjust the light intensity in the short circuit current measurements, the AM 1.5 spectrum has been chosen as a calibration standard in all solar cell's measurements. That spectrum is related to 1000 W/m^2 (Zeman, 2003). The value of I_{sc} depends on the area of the solar cell and to remove that dependence, short-circuit current density (J_{sc}) is usually used instead of I_{sc}.

$$J_{SC} = \frac{I_{SC}}{A} \qquad (\frac{mA}{cm^2}) \qquad\qquad (2.7)$$

where A is the area of the solar cell.

2.5.2   Open-circuit voltage (V_{OC})

It's the potential difference between the electrodes of the DSSC under illumination, with no current is flowing through the external circuit. V_{OC} can be obtained practically when an external load of infinite resistance is attached to the solar cell's terminals. In other words, it is the maximum voltage that a solar cell can deliver. As a related phonemona, the photo-voltage of DSSC equals the difference between quasi-Fermi level of TiO_2 ($E^*_{F,n}$) and the electrochemical potential (E_{redox}) of electrolyte, which is given by

$$V_{photo} = \frac{E^*_{F,n} - E_{redox}}{e} \qquad\qquad (2.8)$$

Increasing the photo-voltage (V_{photo}) will increase the quasi-Fermi level of TiO_2 ($E^*_{F,n}$) of the cell until the value of the quasi-Fermi level of TiO_2 ($E^*_{F,n}$) equals

the value of conduction band edge of the TiO_2 (E_{CB}), $E^*_{F,n} = E_{CB}$. In that case: $V_{photo} = V_{OC}$ and equation (2.8) becomes

$$V_{OC} = \frac{E_{CB} - E_{redox}}{e}$$ (2.9)

where E_{CB} is the conduction band of TiO_2 and E_{redox} is the electrochemical potential of the redox couple. Theoretically, V_{OC} is calculated from equation (2.9) which represents the potential difference between the conduction band edge of the TiO_2 and the redox potential of the I^-/I_3^- pair in the electrolyte (Kuzmych, 2014; Halme, 2002).

2.5.3 Maximum voltage (V_{max})

Maximum voltage corresponds to an optimum point at which the output power of the solar cell is maximum (P_{max}).

2.5.4 Maximum current density (J_{max})

It's equivalent to maximum current obtained at a point of maximum output power (P_{max}) divided by solar cell area.

2.5.5 Fill factor (FF)

It's defined as the ratio between the maximum output power to the product of V_{OC} and Jsc. Fill factor expresses how ideal the solar cell is.

$$FF = \frac{P_{max}}{J_{sc} V_{OC}} = \frac{J_{max} V_{max}}{J_{sc} V_{OC}}$$ (2.10)

2.5.6 Power conversion efficiency (η)

In order to describe the efficiency of a solar cell, the phenomena power conversion efficiency (η) is used, which is the efficiency of converting solar power into electrical power under illumination, and can be defined as :

$$\eta = \frac{P_{max}}{P_{in}} = \frac{J_{max} V_{max}}{P_{in}} = \frac{J_{sc} V_{OC} FF}{P_{in}}$$ (2.11)

where P_{in} is the power of incident radiation which has been adjusted to be 1000W/m^2 at the standard solar spectrum AM 1.5, P_{max} is the maximum electrical power extracted from the solar cell (Zeman, 2003).

2.5.7 Incident photon to current efficiency (IPCE)

It is defined as the ratio of the number of incident photons to the number of charge carriers generated.

$$IPCE = \frac{electrons_{out}}{photons_{in}} = \frac{hc}{e} \frac{J_{sc}}{\lambda.P_{in}} = 1240 \frac{J_{sc}}{\lambda.P_{in}} \tag{2.12}$$

where J_{sc} is the short circuit current density (mA/cm^2), λ is the wavelength (nm), P_{in} is the incident power (mW/cm^2) (Khan, 2013). IPCE can also be expressed as:

$$IPCE = LHE.\phi_{inj}.\eta_{reg}.\eta_{cc} \tag{2.13}$$

where LHE is the light harvesting efficiency, Φ_{inj} is the quantum yield of charge injection , η_{reg} is the dye regeneration efficiency and η_{cc} is charge collection efficiency (Karlsson, 2011). IPCE is often referred to as photocurrent action spectrum or external quantum efficiency.

2.6 Standard measurements

In order to facilate the comparison between different results obtained from DSSCs performance, a solar spectrum of air mass 1.5 (AM 1.5) has been chosen as a calibration standard in solar cells researches, which corresponds to incident power density of 1000 W/m^2 (100 mW/cm^2) at a temperature of 25°C. Figure (2.7) shows the I-V characteristic of such a solar cell in the dark and under illumination.
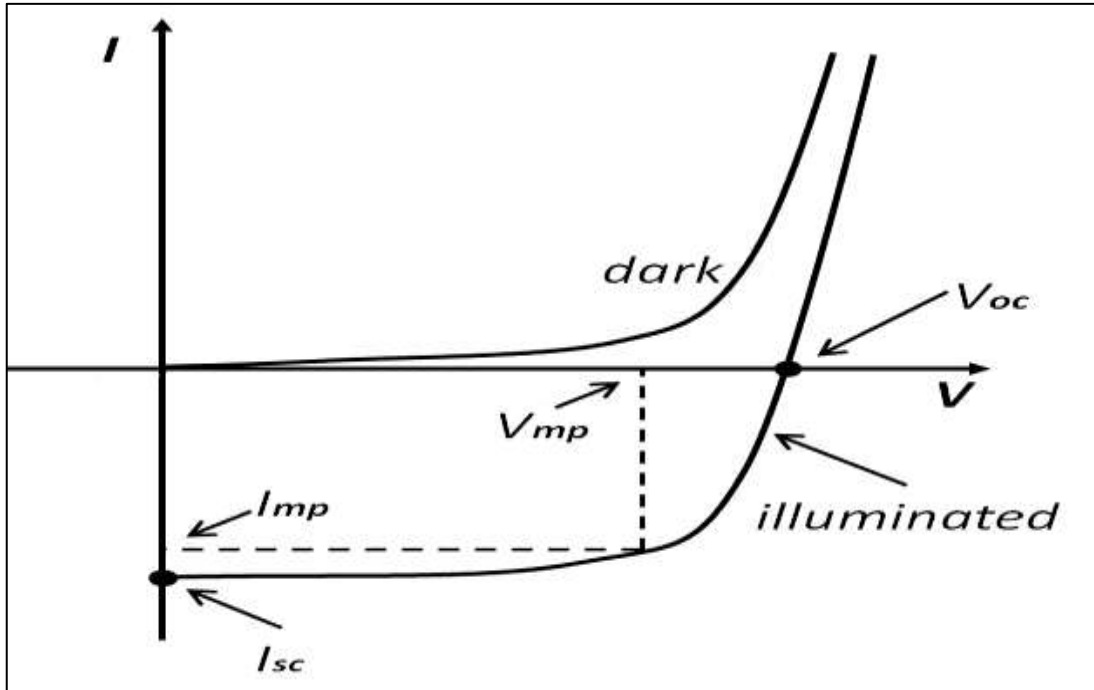
Figure (2.7): I-V characteristic curve in dark and under illumination.

2.7 Equivalent circuit of DSSC

In order to understand the importance of solar cell's parameters in determining the efficiency of the DSSC, a diagram of a simple electric circuit is proposed to mimic processes in DSSC called the equivalent circuit.

2.7.1 Equivalent circuit components

In equivalent circuit, the solar cell is proposed to behave as an ideal diode connected in parallel to current source (I_L) induced by light, shunt resistance (r_{sh}), also known as parallel resistance, which expresses the leakage of current through the solar cell, series resistance (r_s) which expresses the resistance of solar cell materials such as TiO_2, electrolyte and metal contact to current flow. As shown in figure (2.8), I_D is a current flowing through a diode, I_{sh} is shunt current, I is the output current, R_L is the load resistance, r_s is the series resistance and r_{sh} is the shunt resistance (Nelson, 2003).
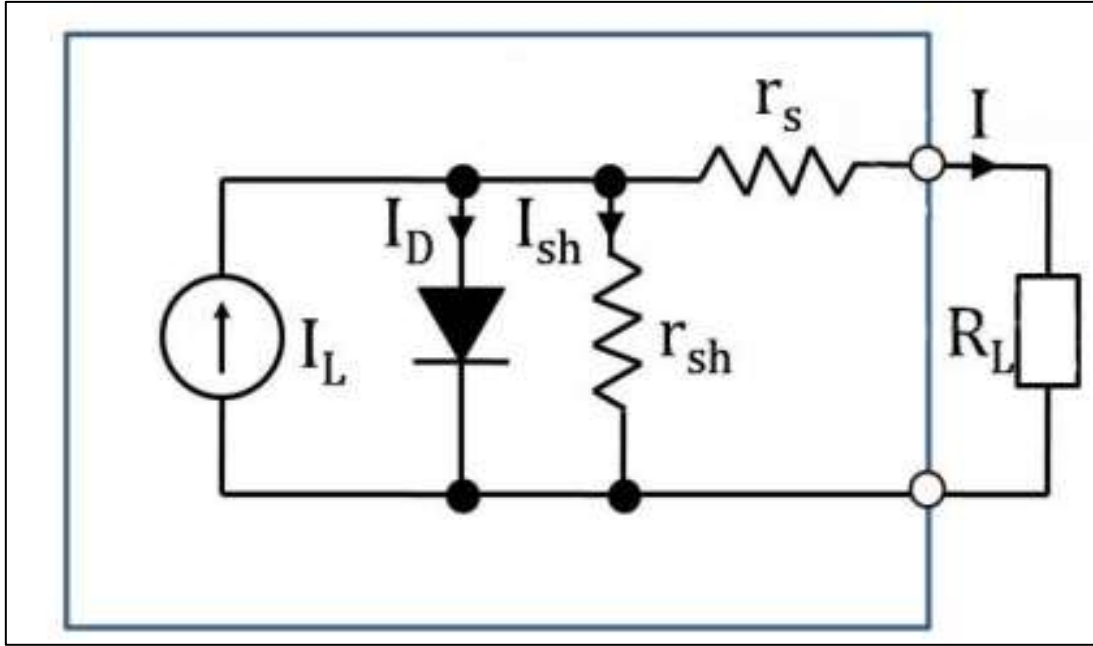
Figure (2.8): Equivalent circuit of DSSC.

2.7.2   Equivalent Circuit Analysis

According to kirchhoff's laws, the output current (I) in the equivalent circuit can be written as:

$$I = I_L - I_D - I_{sh} \tag{2.14}$$

The current passing through a diode (I_D) can be calculated from Shockley diode equation (Shockley, 1976) which is:

$$I_D = I_0\left[\exp\left(\frac{qV_j}{nK_BT}\right) - 1\right] \tag{2.15}$$

where I_0 is the diode saturation current, n is the diode ideality factor, which is a measure of how closely the diode follows the ideal diode equation, q is the elementary charge, k_B is Boltzmann constant, T is absolute temperature, V_j is voltage across both diode and shunt resistor. While the current passing through the shunt resistor is given by Ohm's law:

$$I_{sh} = \frac{V_j}{r_{sh}} = \frac{V + Ir_s}{r_{sh}} \tag{2.16}$$

where V is a voltage across the output terminals. By substituting equations (2.15) and (2.16) into equation (2.14) we get:

$$I = I_L - I_0 \left[\exp\left(\frac{q\ (V + Ir_s)}{nKT} \right) - 1 \right] - \frac{V + Ir_s}{r_{sh}} \tag{2.17}$$

which is known as the single diode model.

It's obvious that the series resistance (r_s) affect negatively the output current of the DSSC. So, for more efficient DSSC, r_s has to be as small as possible. While the shunt resistance (r_{sh}) affect positively the value of output current, for an efficient DSSC the value of r_{sh} has to be as high as possible (Kuzmych, 2014). Generally, the fill factor is influenced by the series resistance, r_s, and the shunt resistance, r_{sh} , of the DSSC.

2.8 Operational differences between DSSCs and the p-n junction solar cells

1- Light absorption and charge transport: Both functions occur in the same material in the p-n junction solar cell, while these functions are seperated in DSSC. The ligh absorption is performed by the dye molecules and the charge transport by the TiO_2 molecules and electrolyte.

2- Charge separation: In a p-n junction solar cell, the charge separation is induced by the electric field across the junction. In DSSCs, it's induced by diffusion and other kinetics as mentioned in section (2.3.3.1).

3- Medium of transporting charge carriers: In p-n junction solar cell, electrons and holes travel in same medium. In DSSC, electrons travel in the TiO_2 network and holes travel in the electrolyte, both in different directions (Halme, 2002).

2.9 State of art

The impact success in DSSCs field is reffered to Grätzel and O'Regan in 1991. They used porous TiO_2 films and a ruthenium–polypyridine complex dye (O'Regan & Grätzel, 1991). Following this success, a conversion efficiency of 10.4% was

achieved using the black dye as a photo-sensitizer where the spectral absorption of the complex dye was extended into the near-infrared region (Nazeeruddin et al., 2001; Grätzel, 2001).

Thereafter, researches have focused on modifying the various components of DSSC such as modifying the working electrode, counter electrode, sensitizers and electrolyte. Several methods have been utilized in modifying the structure of working electrode (WE). For example, S. Ito et al. have reported a conversion efficiency over 10% by modifying the working electrode with the three following techniques, the first technique was the pre-treatment of the WE with $TiCl_4$ which improved the adhesion and the mechanical strength of the nano-crystalline TiO_2 layer, while the second techniques was varying the thickness of the TiO_2 layers and the third technique was adding an anti-reflecting film (ARF) to the electrode's surface which enhanced the IPCE of the DSSC device to reach up to 94% at wavelengths close to the absorption maximum of the sensitizer (Ito et al., 2008). C. Chou et al. have investigated the applicability of TiO_2/Au and TiO_2/Ag composite particles in forming a film used as photo-electrode in the DSSC, they found that the power conversion efficiency (η) of the DSSC with working electrode modified with of TiO_2/Au and TiO_2/Ag films exceeded that of the conventional DSSC (Chou et al., 2009).

Studies of modifying the counter electrode (CE) in the DSSCs were also continued, for example, K. Lee et al. have employed a layer of poly(3,4-ethylenedioxythiophene) (PEDOT) on the FTO substrate to modify the counter electrode in the platinum-free DSSCs, where the resulting PEDOT counter electrodes showed excellent catalytic behavior in DSSC leading to good cell performance (Lee et al., 2010).

Researches on sensitizers gains a great attention due to it's important role in the DSSCs. For example, different ruthenium based organic dyes such as N3, N719 and Black dye were used as photo-sensitizers in DSSCs and efficiencies of more than 11% were obtained (Nazeeruddin et al., 2001). Moreover, new sensitizers were designed and applied in DSSCs to promote the absorption of the visible spectrum such as the iminocoumarin dyes (2a–c and 3a–c) which were synthesized by

31

introducing carboxyl and hydroxyl anchoring groups onto the dyes structure where the results showed that these iminocoumarin dyes are suitable as light-harvesting sensitizers in DSSC application (Kandavelu et al., 2009).

Other studies have reported an efficiency of about 0.12% when the used photo-sensitizer was the eosin Y, where the short circuit current density was 0.25 mA/cm^2 and the open circuit voltage was 0.81V (Das et al., 2016).

For the electrolyte modification, a recent Zn-based dye and Co-based electrolyte pair have been developed and their efficiency has exceeded 12% (Yella et al., 2011).

Nowadays, efforts are being continuaed in the research and development of low-cost dye-sensitized solar cells (DSSCs), where the record conversion efficiency for the DSSCs currently stands at the range 12–13% (Mathew, 2014).

Chapter 3
Materials and Experimental

Chapter 3

Materials and Experimental

In this chapter, a brief description of main instruments used in characterizing DSSC is presented such as UV-Vis spectroscopy which examines the optical properties of the dye and the I-V measurement system that measures the current voltage- characteristics of the DSSCs and the cell efficiency. Materials and techniques used in the DSSCs preparation are also discussed.

3.1 Experimental techniques

A description of techniques and instruments used in the work are presented in this section.

3.1.1 UV-VIS Spectroscopy

Ultraviolet and visible (UV-Vis) absorption spectroscopy can be used to measure the absorbance of ultraviolet or visible radiation of a sample. Absorbance can be measured at a single wavelength or over a range of wavelengths in the spectrum. The UV region ranges from 190 to 400 nm and the visible region from 400 to 800 nm. Usually, the sample used to measure its absorbance is in liquid state, since only small numbers of absorbing molecules are required. The sample is dissolved in a solution (Rouessac& Rouessac, 2013). In the spectrophotometer, two flat transparent containers exist, called cuvettes. The sample is held in one cuvette, known as the sample cuvette, and the reference cuvette which contains the solvent in which the sample is dissolved, the reference cuvette known as the blank. The light source in the spectrometer is a combination of a hydrogen or deuterium discharge lamp which covers the ultraviolet range and a tungsten filament which covers the visible range. In this way, the light source can cover the range of visible and near ultraviolet radiation (200 nm– 800 nm).
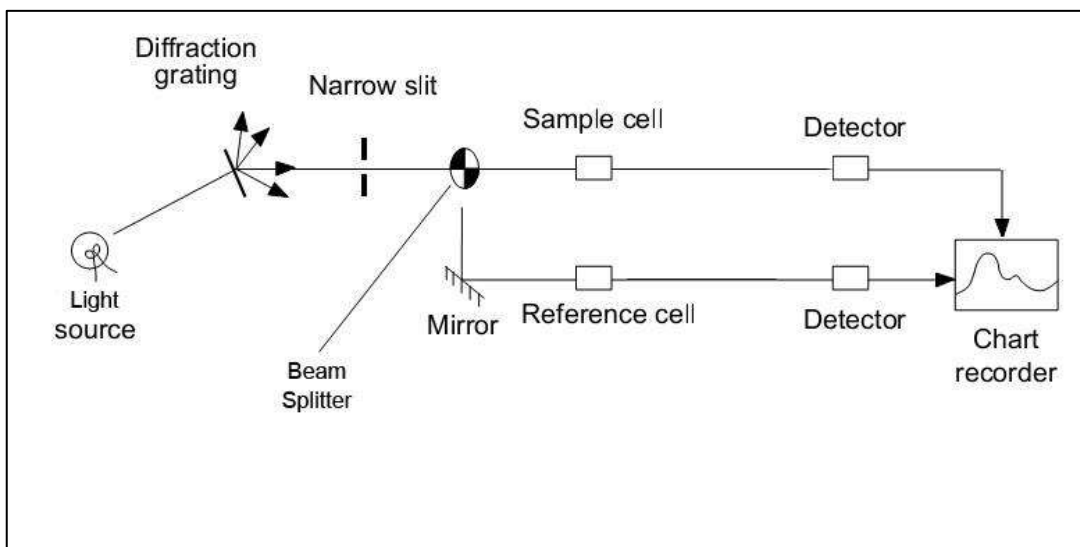
Figure (3.1): Schematic representation of UV-visible spectrophotometer.

A schematic representation of UV-visible spectrophotometer is shown in figure (3.1). The technique of measuring absorbance of a sample is as follow: A light beam from the light source passes through a diffraction grating which separates the radiation according to its wavelengths, followed by a narrow slit that acts as a monochromator that narrows the waveband of radiation. Each single wavelength in the radiation is split into two parts of the same frequency and intensity, the first part passes through the sample cuvette and the second part passes through the reference cuvette. Then, the radiation passed through the sample cuvette (I) and through the reference cuvette (I_o) can be detected by a photodiode, that converts photons of radiation into tiny electrical currents. By comparing the currents generated by the sample and the reference beams, a spectrum of the sample is produced, where the spectrum is plotted as absorbance against wavelength (nm) in the UV and visible regions, figure (3.2).
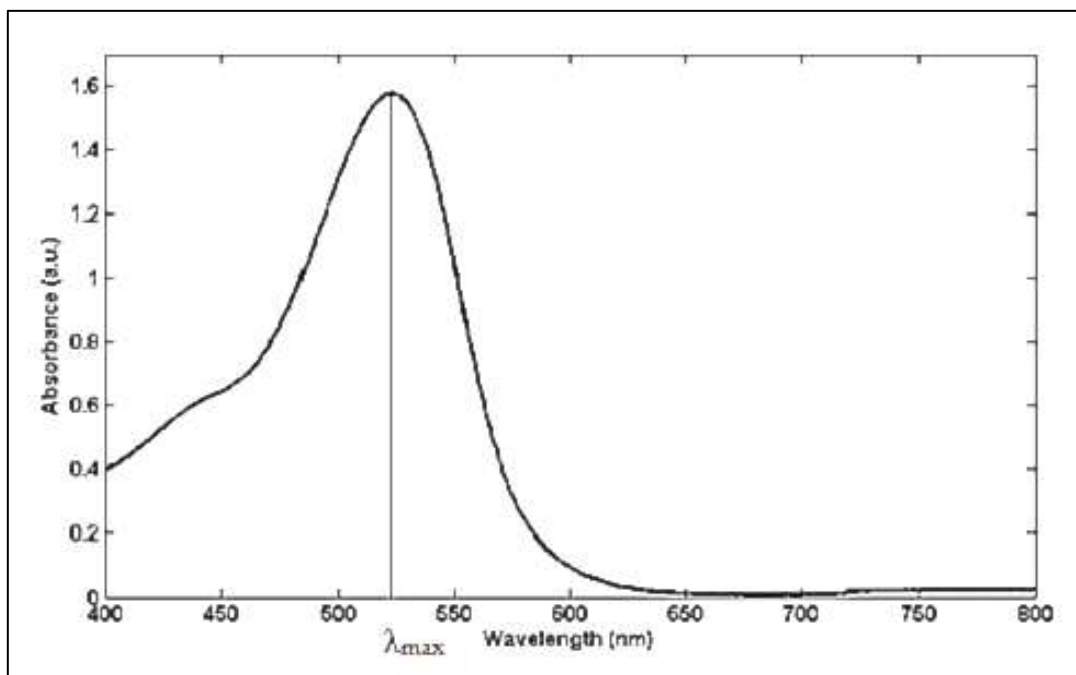
Figure (3.2): Absorption of light by dye using UV-Vis spectroscopy.

Physically, the way of expressing absorbance results from two approaches, The first approach is in terms of I and I_o which is as follow:

Supposing that I_o is the intensity of the incident radiation which equals the radiation intensity transmitted through the reference cuvette (assuming that the solvent has a slight absorbance of the incident radiation), and I is the intensity of the transmitted radiation through the sample. The ratio of transmitted intensity (I) to the incident intensity is known as the transmittance (Meyer& Jürgen, 1989).

$$T = \frac{I}{I_o} \tag{3.1}$$

The absorbance (A) is defined as follows:

$$A = -\log_{10} T \tag{3.2}$$

Substituting equation (3.1) into equation (3.2), the absorbance (A) becomes:

36

$$A = -\log_{10}\frac{I}{I_o} = \log_{10}\frac{I_o}{I} \tag{3.3}$$

While the second approach results from Beer's law and Lambert's law, where the absorbance of a sample depends on two assumptions:

1- The absorbance is directly proportional to the concentration (c) of the sample molecules used in the experiment, Beer's law.

$$A \propto c \tag{3.4}$$

2- The absorbance is directly proportional to the length of the light path (l), which is equal to the width of the cuvette, Lambert's law.

$$A \propto l \tag{3.5}$$

Combining equations (3.4) and (3.5), we get:

$$A \propto cl \tag{3.6}$$

Converting the proportionality of the last equation into an equality by including a proportionality constant (ϵ), we get:

$$A = \epsilon cl \tag{3.7}$$

Which is the common formula of the Beer-Lambert Law, where ϵ is the molar absorption coefficient of the material and having the units $mol^{-1}dm^{3}cm^{-1}$, c is the concentration of the absorbing sample in $mol\ dm^{-3}$ and l is the length of the light path or the width of the cuvette, in cm.

Combining equations (3.3) and (3.7), the absorbance becomes:

$$A = -\log_{10}\frac{I}{I_o} = \log_{10}\frac{I_o}{I} = \epsilon cl \tag{3.8}$$

where A has no units. All absorption spectra of this work were measured by GENESYS 10S UV-Vis spectrophotometer, figure (3.3).

Figure (3.3): GENESYS 10S UV-Vis spectrophotometer.

3.1.2   I-V measurement system

In order to investigate the performance of the assembled DSSC, a solar simulation system is equipped. This system, illustrated in figure (3.4), consists of light source of power intensity $1000W/m^2$ that satisfying the standard condition of AM1.5, Autolab device which can be connected to the electrodes of the cell under investigation and a computer that is connected to the Autolab through special wires. To activate that system, a special program should be installed on the computer, it's known as Autolab NOVA software. NOVA is the data reading and analysis software package for all Autolab functions. The most important techniques available in NOVA are:

1- Cyclic and linear sweep voltammetry.
2- Impedance spectroscopy.
3- Voltametric analysis.
4- Chrono methods.

In this system, the I-V characteristic curve of the assembled DSSC was investigated by running the function linear sweep voltammetry potentiostatic in

NOVA program, where the applied potential ranged from -0.7V to 0.7V. The main factors such as short circuit current (I_{SC}), open circuit voltage (V_{OC}), fill factor (FF), maximum current (I_{max}), maximum voltage (V_{max}), maximum power (P_{max}) and efficiency (η) were calculated from the resulting data and all resulting data were saved in text files to be used in the study.
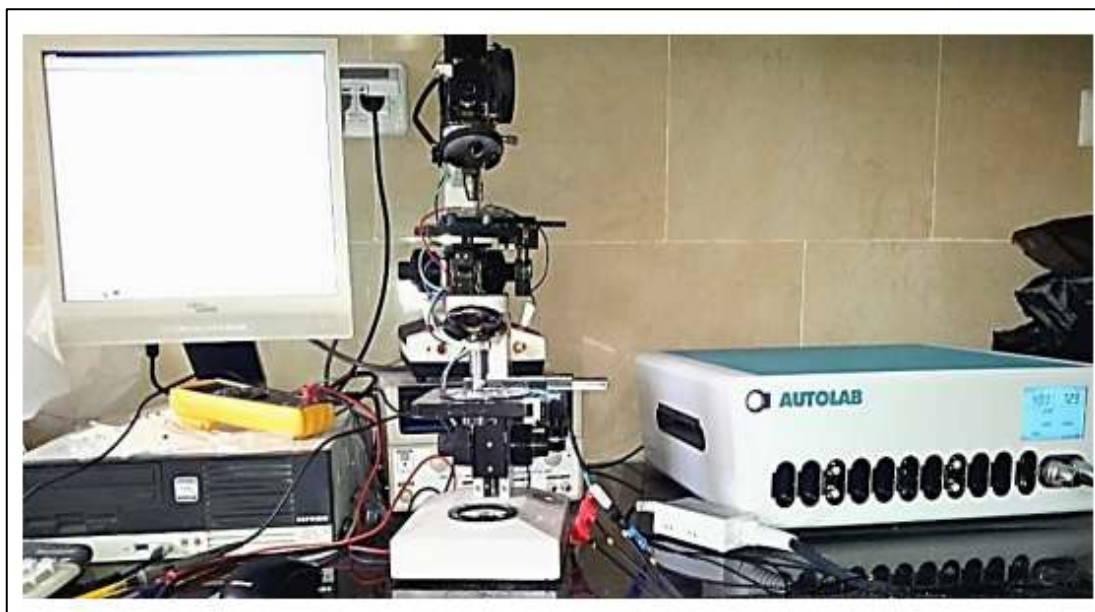
Figure (3.4): Autolab AUT 85276 Potentiostat- Gelvanostat with frequency response analyzer FRA 32 Module.

3.2   Device fabrication (assembly)

This section presents the materials used in fabricating the DSSC device. The conditions of each material are also described.

3.2.1   Materials used in preparing the DSSC device

1- Transparent conducting oxide substrates in the form of fluorine-doped tin oxide (FTO) with sheet resistance 15 $\Omega/\square$, and transmission >80% (Xinyan Tech. Ltd, Hong Kong).

2- TiO_2 nanoparticles with a diameter of about 25 nm (US Research Nanomaterial, Lnc, USA).

3- Eosin Y dye as a photo-sensitizer, purchased from Sigma-Aldrich.

4- Platinized counter electrode formed by adding a thin layer of platinum on FTO substrate.

5- Liquid electrolyte consisting of ACN solvent and (I^-/I_3^-) redox couple.

3.2.2 FTO substrates preparation

The FTO glass substrates were scratched with a glass cutter into area of 2 x 2 cm^2. The glass was sonicated in 10 wt.% NaOH solution for 10 minutes and rinsed thoroughly in water, followed by a sonication bath for 15 minutes in distilled water and then rinsed with water and ethanol. Finally, they were dried in an oven at 60°C for 30 minutes. The sheet resistance of the FTO conductive glass was measured and found to be 15-20 $\Omega/\square$.

3.2.3 Photo-electrode preparation

TiO$_2$ paste was prepared by mixing 1gm of TiO$_2$ nano-powder (25nm) with 2 gm of polyethylene glycol in agate mortar for 20 minutes to get a homogeneous paste. Two of the side edges of the FTO substrates were covered with a layer of adhesive tape to control the thickness of the TiO$_2$ films. By doctor blading method, the paste was spread on the FTO substrates by rolling a rod coater onto the FTO substrates along the tape spacer in order to obtain films each of area 0.25 cm^2, the technique is illustrated in figure (3.5). After spreading the paste, the films were left to dry before removing the tape. The prepared films were sintered in the furnace at 450℃ for 30 minutes, where the temperature was raised gradually to 450℃. After sintering, the films were cooled gradually to 60℃ and the films were ready for dying process.
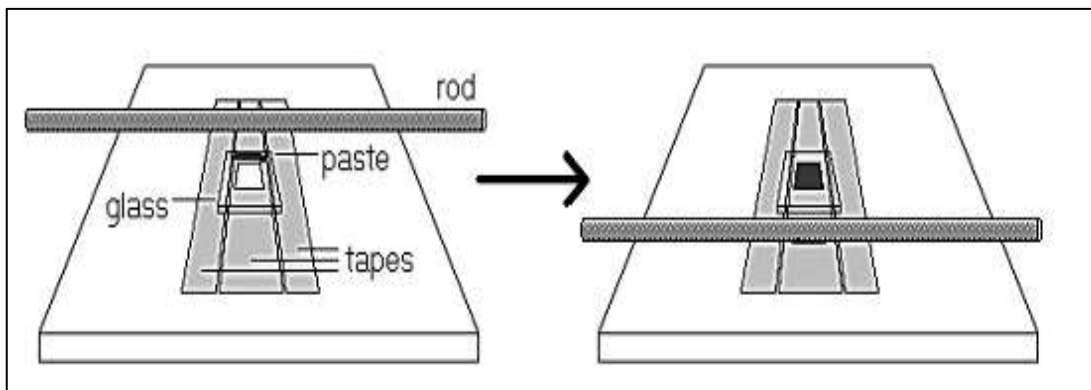
Figure (3.5): An illustration of doctor blading technique.

3.2.4 Preparing the photo-sensitizer and films dyeing

Eosin-Y ($C_{20}H_8Br_4O_5$) is an organic dye with a molecular weight of 647.89 gm/mol. It was used as a photo-sensitizer in the fabricated DSSC. The molecular structure of eosin Y is shown in figure (3.6).
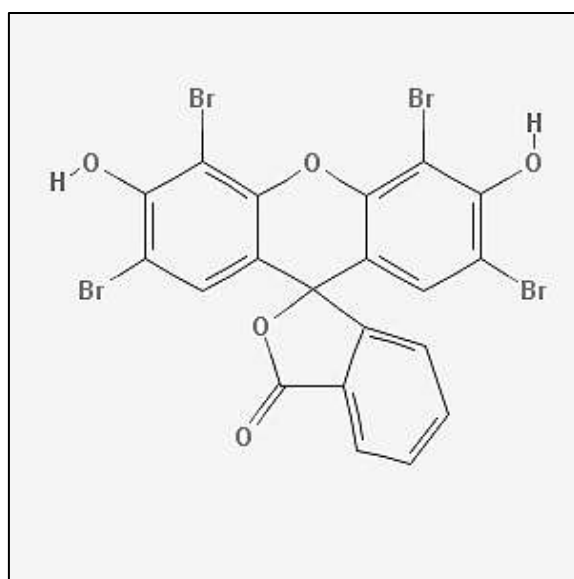
Figure (3.6): The molecular structure of eosin Y

For dyeing process, a solution of concentration 0.32 mM was prepared by dissolving 0.04 gm of eosin Y in 200 ml ethanol. The prepared TiO_2 films were heated for 10 minutes at 60℃ in the furnace to ensure the evaporation of any condensed water on the films, since the condensed water may reduce the amount of adsorbed dye onto the films. After that, these films were immersed in the dye

41

solutions for different times ranged from 3 hours to 24 hours. After dyeing, the films were rinsed with ethanol to remove excess dye and dried on the hot plate for 3 minutes. Then, the dyed TiO_2 films are ready to be used as a photo-electrode in the DSSC assembly.

3.2.5   Preparing liquid electrolyte

Liquid electrolyte was prepared by dissolving 0.66 gm of lithium iodide (LiI) and 0.63 gm of iodine (I_2) in a beaker containing 2ml of acetonitrile (ACN) and 8ml of propylene carbonate (p- carbonate). The solution was heated for 20 minutes on the hot plate with stirring, and then the electrolyte was kept in a black bottle to be used later in the DSSC device.

3.2.6   DSSC assembly

The prepared parts of DSSC were assembled together forming the DSSC device, where the dyed FTO side was put onto a platinized counter electrode with a slight offset between the two electrodes. The two electrodes formed a sandwich configuration, where the upper part was the dyed film (the anode) and the lower part was the counter electrode. This sandwich form was connected to external configuration including a light source of 1000 watt intensity, a multi-meter used to indicate the output voltage of the DSSC and the autolab device which gives the I-V measurements of the fabricated cell. The two electrodes were pressed on each other till a high voltage value was obtained on the multi-meter screen. Finally, The electrolyte redox (I^-/I_3^-) was spread through the vicinity between the two electrodes using a micropipette. By turning on the lamp (1000W), the DSSC device was working and the I-V measurements were done by the Autolab.

3.2.7   Synthesis of eosin Y derivative

A solution of eosin Y derivative was prepared by mixing the eosin Y solution with a solution of phenylhydrazine hydrochloride ($C_6H_5NHNH_2 \cdot HCl$) in a molar ratio 1:1. The molecular weight of phenylhydrazine hydrochloride is 44.6 gm/mol and molecular structure is presented in figure (3.7). A precursor solution of concentration 5mM was

prepared by dissolving 0.014 gm of the phenylhydrazine hydrochloride in 20 ml of distilled water, the precursor solution was kept to be used in preparing the solution of eosin Y derivative. To get the ratio of 1:1 in synthesizing the eosin Y derivative, 1 ml of the phenylhydrazine hydrochloride solution was added to 15 ml of the eosin Y solution with heating on the hot plate at 60℃ for 10 minutes. The resulting mixture was the eosin Y derivative solution which was used in dyeing the TiO_2 films.
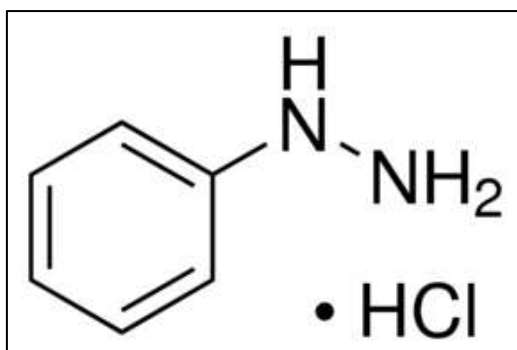
Figure (3.7): The molecular structure of phenylhydrazine hydrochloride.

3.2.8   Adding zinc oxide (ZnO) blocking layers

In order to prevent injected electrons in the TiO_2 electrode from recombining with both the oxidized dye and the tri-iodide in the electrolyte, losses due to recombination, blocking layers of ZnO were introduced at the TiO_2/electrolyte interface. These layers act as an energy barrier (figure 3.8) that reduces the recombination of electrons with oxidized dye molecules or with I_3^- in the electrolyte (Zhang et al., 2009). The conduction-band edge of the energy barrier should be more negative than that of the TiO_2, so the transport of electrons in the reverse direction can be blocked by the energy barrier (Chou et al., 2012).
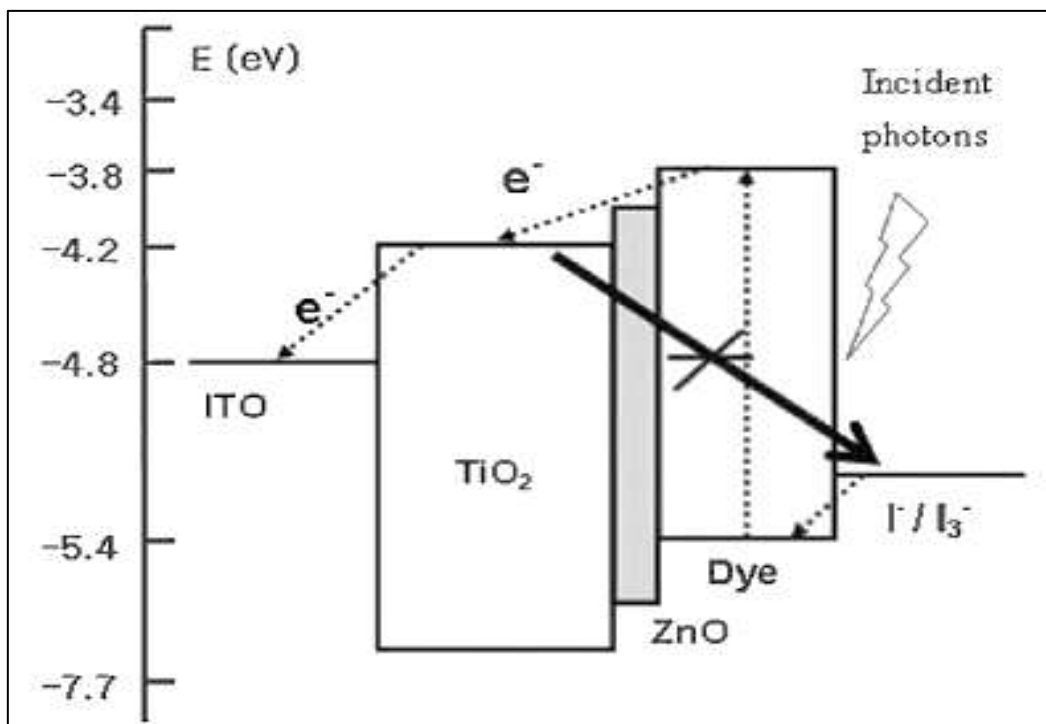
Figure (3.8): ZnO layers act as energy barrier blocking electrons transport in the reverse direction.

In this work, ZnO layers were introduced in the DSSCs in the following two manners:

1- **ZnO upper layers:** A simple dip coating method was used to fabricate ZnO coated TiO_2 electrode by immersing the FTO glass substrate with TiO_2 films in a solution of zinc nitrate hexahydrate ($Zn(NO_3)_2$. $6H_2O$) and ethanol, where the TiO_2 films were immersed in the precursor solutions of different concentrations for 2 minutes at temperature of 60℃, then the films were sintered at 450℃ for 30 minutes and finally were dyed by eosin Y dye. The effect of the concentration of $Zn(NO_3)_2$. $6H_2O$ in forming a blocking upper layer on the TiO_2 electrode in the DSSC was investigated by the I-V measurement system.

2- **ZnO under-layers:** Layers of ZnO was introduced at the FTO/ TiO_2 interface, where the FTO glass substrates were immersed in solutions of zinc nitrate hexahydrate ($Zn(NO_3)_2$. $6H_2O$) and ethanol with different concentrations for 2 minutes at temperature of 60℃, then the substrates were sintered at 450℃

for 30 minutes to ensure the formation of ZnO layers on the substrates. Finally, the substrates were coated with TiO_2 films and dyed with eosin Y dye. The effect of adding ZnO under layers on the DSSCs performance was investigated by the I-V measurement system, where different concentrations of $Zn(NO_3)_2$. $6H_2O$ were also investigated.

3.2.9 Open-circuit voltage decay (OCVD) measurement

Open-circuit voltage decay (OCVD) technique has been employed to study the electron lifetime (τ_n) in DSSC. The OCVD measurement can be performed by the autolab device, through NOVA program. The procedure chrono potentionmetry ($\Delta t>$ 1ms) is chosen while the light source is illuminated at the DSSC, after a few seconds, the illumination was interrupted and a curve of photo-voltage decay with time was observed on the screen, as illustrated in figure (3.9).
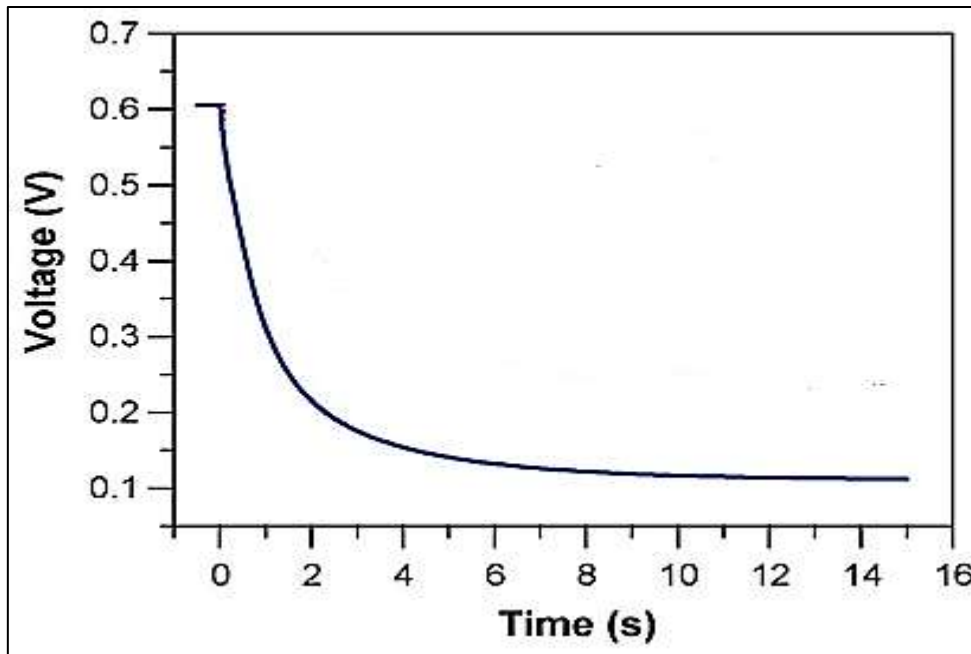
Figure (3.9): Open-circuit voltage decay curve of the DSSC.

From the OCVD experiment, the electron lifetime (τ_n) was calculated by taking the inverse of the derivative of the decay curve using equation (3.9).

$$\tau_n = - \frac{K_B T}{e} \left(\frac{dV_{OC}}{dt}\right)^{-1}$$

(3.9)

45

where k_B is Boltzmann constant, T is absolute temperature, e is the positive elementary charge and dV_{oc}/dt is the derivative of the open-circuit voltage (Zaban et al., 2003).

3.2.10 Dye uptake (desorption method)

Determining of the amount of dye adsorbed on the TiO_2 films were performed by the UV-Vis spectrophotometry, where a solution of 0.1M NaOH was used in the desorption method. The dyed films were immersed in 3.5ml NaOH solution for 24 hours ensuring a complete desorption of the dye from TiO_2 films. After that period, the solutions of desorbed dye were kept in small cups in the dark to be analyzed. As a first step in calculating the dye uptake by the UV-visible spectrophotometer, a baseline was performed using a cuvette filled with pure NaOH solution. By running the baseline, the absorbance of NaOH was subtracted from the absorbance of the dye solution before plotting, so the absorbance which was plotted by the device was referred to the dye molecules only not to the NaOH solution in which the dye was desorbed.

After running the baseline, dye solutions of different known concentrations were prepared using eosin Y dye to be used as a reference dye solution in measuring process of the device. The absorbances of these reference solutions were measured each time and recorded at a spectral wavelength of 516.8 nm. That value is referred to a wavelength at which the peak was observed where the solvent was the sodium hydroxide. Plotting each concentration of the reference solutions as a function of absorbance, a straight line was obtained and the slope was calculated.

The last step was measuring absorbance of the desorbed dye solution where 1.5 ml of desorbed dye solution was put in the cuvette and running the device and the absorbance of the dye at the wavelength 516.8 nm was recorded to be used in calculations. By substituting the absorbance value of the dye in the resulting slope relation, the concentration of desorbed dye from TiO_2 films was determined.

Chapter 4

Results and Discussion

Chapter 4

Results and Discussion

In this chapter, experimental results will be presented and discussed in detail, including determination of the best dyeing time and the amount of the dye adsorbed onto TiO_2 films. In addition to determining the lifetime of electrons through the open-circuit voltage decay (OCVD) measurement. The effect of changing the pH of the dye solution on the DSSC efficiency will be studied. Finally, introducing blocking layers of ZnO nano-particles will be investigated where the blocking layers will be introduced as upper and under layers.

4.1   Characterization of dye solar cell sensitized with eosin Y

The optical properties of the assembled DSSCs, which were dyed for over one night, were investigated by GENESYS 10S UV-Vis spectrophotometer available at the   Islamic university of Gaza (IUG), Gaza-Palestine. Figure (4.1) shows the absorption spectrum of eosin Y dissolved in ethanol, which has a main peak at wavelength of 525 nm.
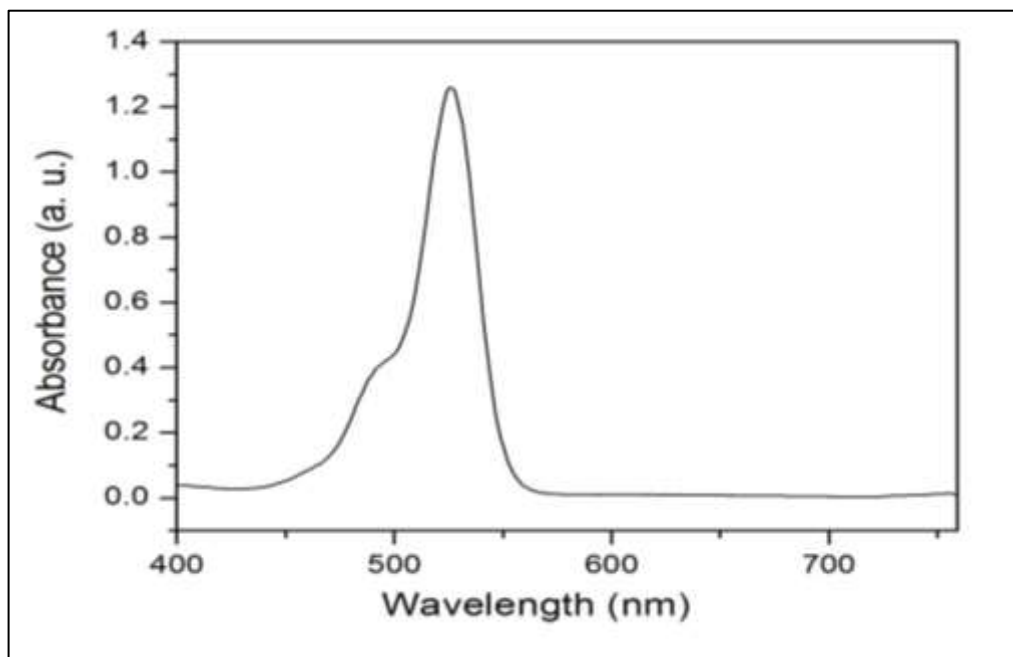
Figure (4.1): Absorption spectrum of eosin Y dissolved in ethanol.

The kubelka-munk measurement, figure (4.2), shows that the absorption spectrum of the adsorbed dye onto TiO_2 film has its main peak at wavelength of 531 nm. The shift of the main peak to a longer wavelength after soaking the TiO_2 electrode in the dye solution resulted from the interaction between the TiO_2 molecules with the dye.
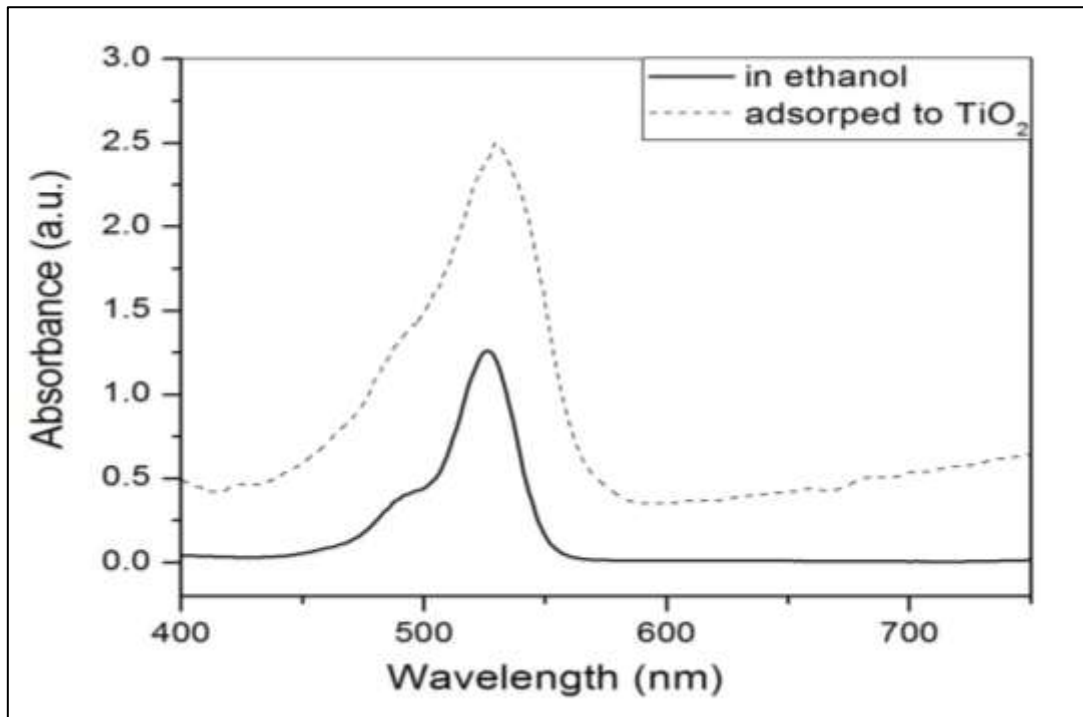
Figure (4.2): Kubelka-munk measurement of eosin Y adsorbed onto TiO_2 film.

The J–V characteristic curve of the assembled DSSC is shown in figure (4.3), where the short circuit current density (J_{SC}) was 0.47 mA/cm^2 and the open circuit voltage (V_{OC}) was 0.398 V, while the efficiency of the DSSC was 0.05% .
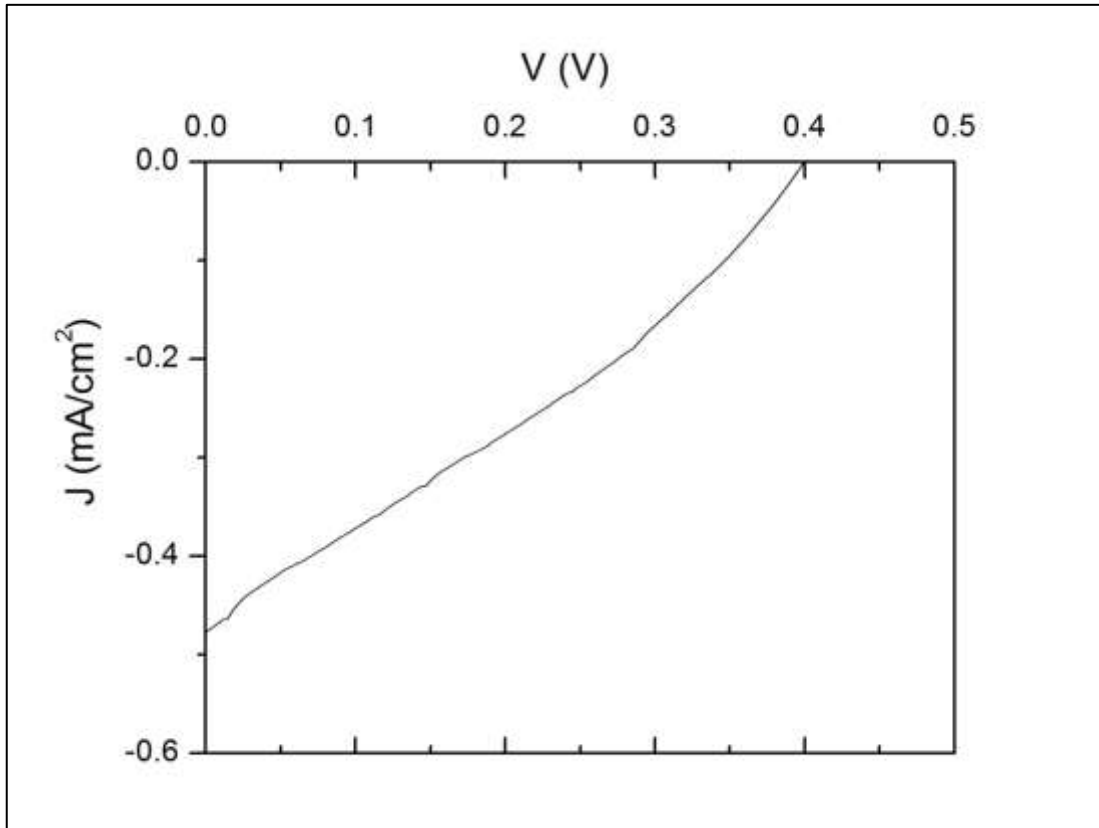
Figure (4.3): Current density (J) versus voltage (V) characteristic curve of the DSSC sensitized with eosin Y.

4.2   Duration of dyeing

The time it takes for the dye to fully cover the TiO$_2$ films is known as the duration of dyeing, it usually ranges from 1 hour to 24 hours. In this work, the effect of dyeing duration on the performance of the assembled DSSCs was investigated.

4.2.1   Experiment

The influence of the periods 1 hour, 3 hours, 6 hours and 24 hours was investigated. The TiO$_2$ films were immersed in 0.32 mM eosin Y solutions for the defined periods in the manner mentioned in section 3.2.4.

4.2.2 Results and discussion

The J–V characteristics of DSSCs which were dyed for different times is shown in figure (4.4). The short circuit current density (J_{SC}) has a maximum value of 0.82 mA/cm^2 when the dyeing time was 3 hours and an open circuit voltage has its maximum value of 0.46 V at that time too. The main photovoltaic parameters for dyeing durations are presented in table (4.1), the fill factors (FF) has its maximum value when the dyeing duration was 24 hours while the efficiency (η) has its maximum value when the dyeing duration was 3 hours.
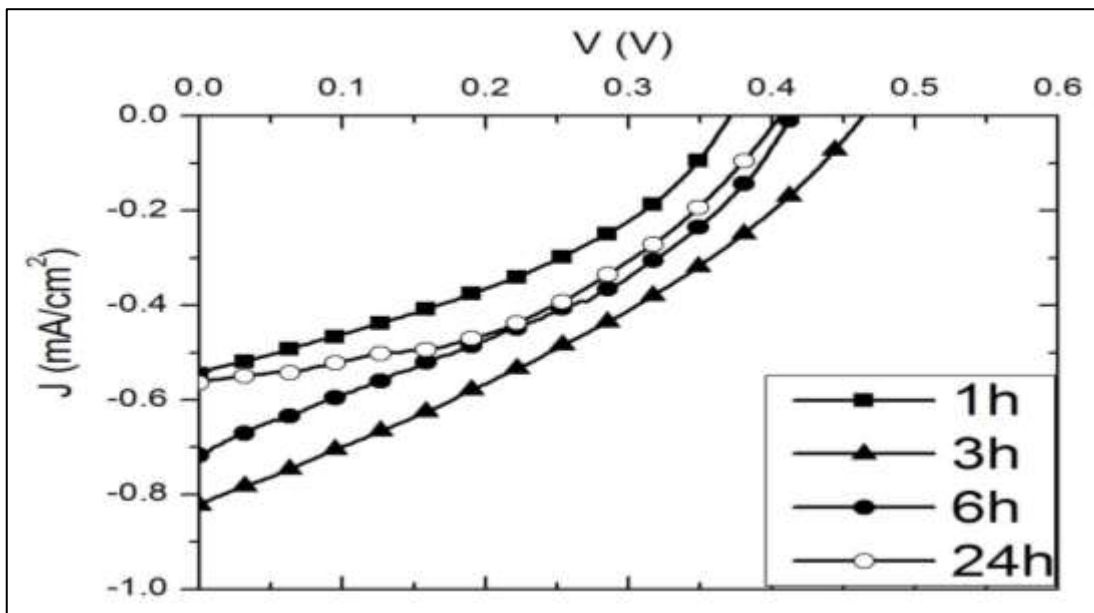
Figure (4.4): Current density (J) versus voltage (V) characteristic curves for different dyeing durations of the DSSCs.

Table (4.1): Effect of dyeing duration on the photovoltaic parameters of the DSSCs.

Dyeing duration (h)	J_{SC} (mA/cm^2)	V_{OC} (V)	J_m (mA/cm^2)	V_m (V)	FF	η %
1	0.54	0.370	0.29	0.240	0.34	0.07
3	0.82	0.460	0.43	0.290	0.33	0.12
6	0.71	0.413	0.37	0.280	0.35	0.10
24	0.56	0.405	0.36	0.265	0.42	0.09

The power curves as a function of the photo-voltage for different dyeing durations of the DSSCs are shown in figure (4.5).
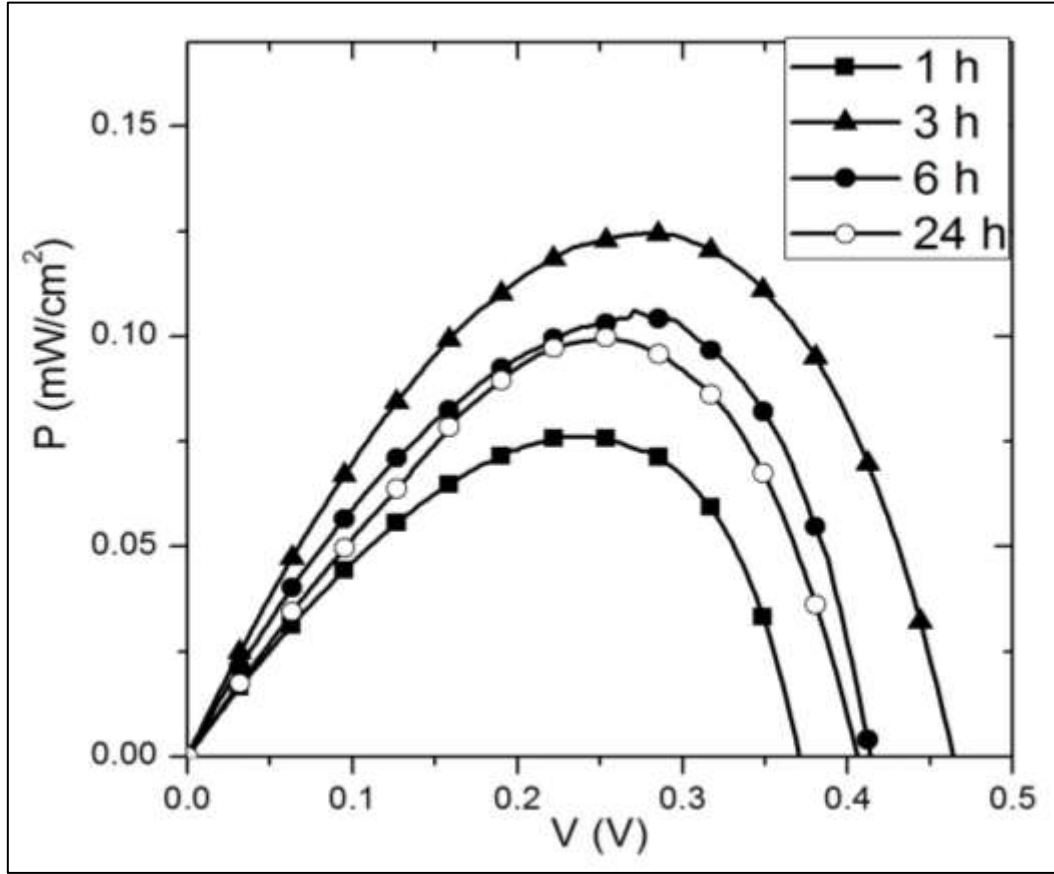
Figure (4.5): Power (P) versus voltage (V) characteristic curves for different dyeing durations of the DSSCs.

4.3 Open-circuit voltage decay (OCVD) measurement

4.3.1 Experiment

Open circuit voltage decay curve was determined by the procedure mentioned in section (3.2.9) and the lifetime of electrons is given by

$$\tau_n = - \frac{K_B T}{e} \left(\frac{dV_{OC}}{dt}\right)^{-1} \tag{4.1}$$

By substituting both the derivative of the open-circuit voltage (dV_{oc}/dt) and the constant $\frac{K_B T}{e}$, which equals 0.25455 J/C, into equation (4.1), the lifetime of electrons was represented as a function of the V_{OC} (Zaban et al., 2003).

4.3.2 Results and discussion

The open-circuit voltage decay curve of the DSSC is shown in figure (4.6), where the decay of the photo-voltage reflects the decrease of the electron concentration at the FTO surface, which is mainly caused by the charge recombination. Figure (4.6) shows that the device has a steady state open-circuit voltage (V_{OC}= 0.376V) for 12.5 seconds, after that period, the electrons start to recombine with the tri-iodide ions (I_3^-) on the TiO$_2$ surface within 3.5 seconds.
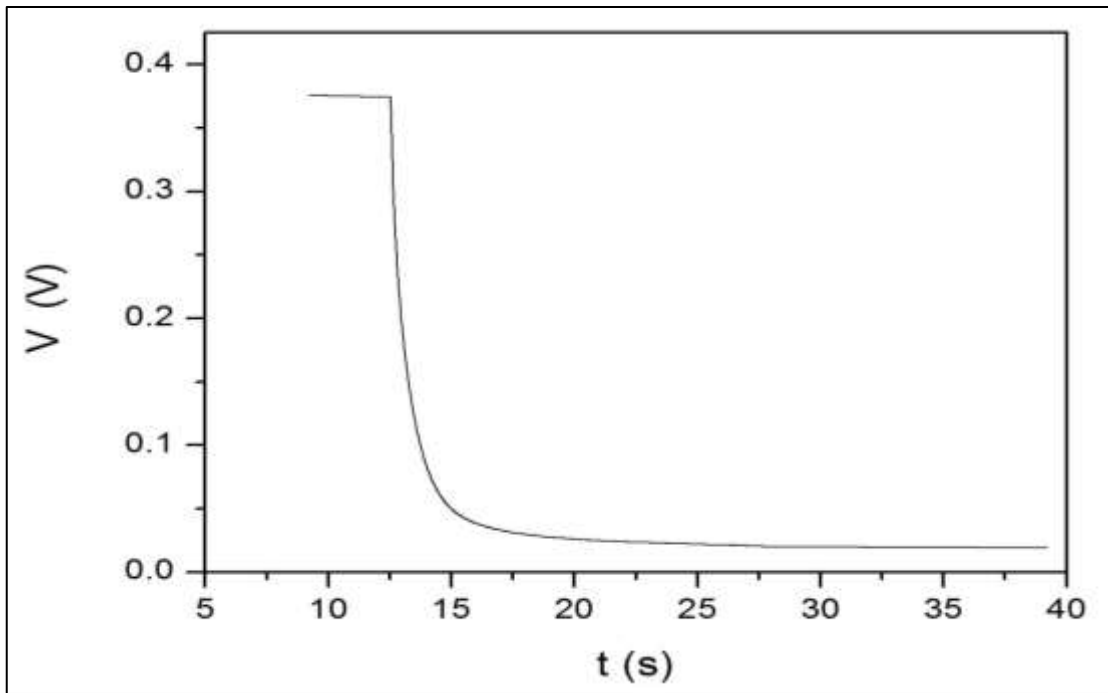
Figure (4.6): Open-circuit voltage decay curve of the DSSC.

The lifetime of the electrons as a function of the open circuit voltage (V_{OC}) is shown in figure (4.7), where electron lifetime (τ_n) can quantify the range of electron recombination with the redox electrolyte in the DSSC. The figure shows that the lifetime of electrons is 3 seconds before being annihilated by the redox electrolyte.
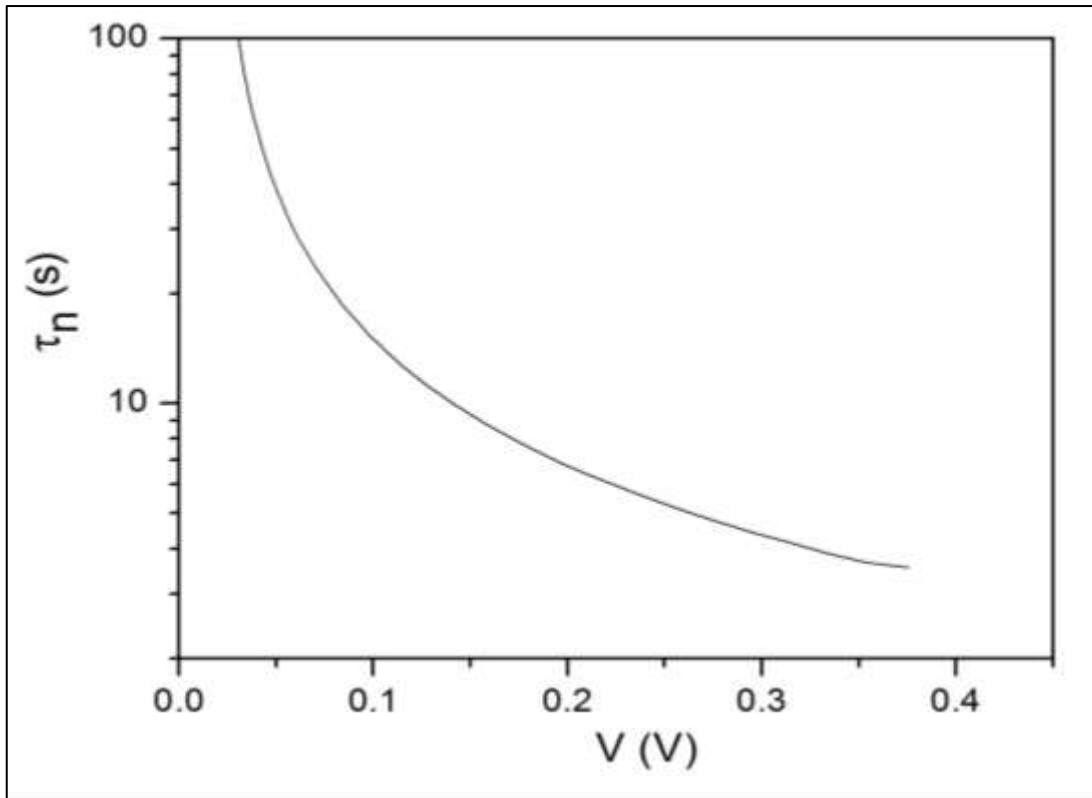
Figure (4.7): Electron lifetime versus the open-circuit voltage (V_{OC}) of DSSC.

4.4 Determining the amount of the dye adsorbed onto TiO$_2$ films

4.4.1 Experiment

Determination of the amount of eosin Y dye adsorbed on the TiO$_2$ films in the assembled DSSCs was carried out by the desorption method. The dyeing durations of 3 hours and 24 hours were chosen to investigate how much dye was adsorbed on the TiO$_2$ films during these durations. Four different known concentrations of the dye solution were used as a reference dye solution where the absorbance of each concentration was determined by running the UV-visible spectrophotometer that procedure resulted in a table of two columns included the concentration of the dye solution and the absorbance of each concentration. The absorbance versus dye

concentration was plotted and the concentrations of the dye desorbed from the TiO_2 films for the dyeing durations 3 hours and 24 hours were determined according to the slope of the plotted relation.

4.4.2   Results and Discussion

Absorbance as a function of the dye concentration is shown in figure (4.8). The absorbance of the desorbed dye solutions resulted from dyeing durations of 3 hours and 24 hours were 0.152 and 0.184 respectively, where the dye concentrations of the two durations, which are the x- coordinates, corresponded to the y- coordinates 0.515 μM and 0,525 μM respectively. In other words, when the TiO_2 films were dyed for 3 hours, the concentration of the adsorbed dye on each TiO_2 film was 0.515 μM and when they were dyed for 24 hours, the concentration of the adsorbed dye was 0.525 μM.
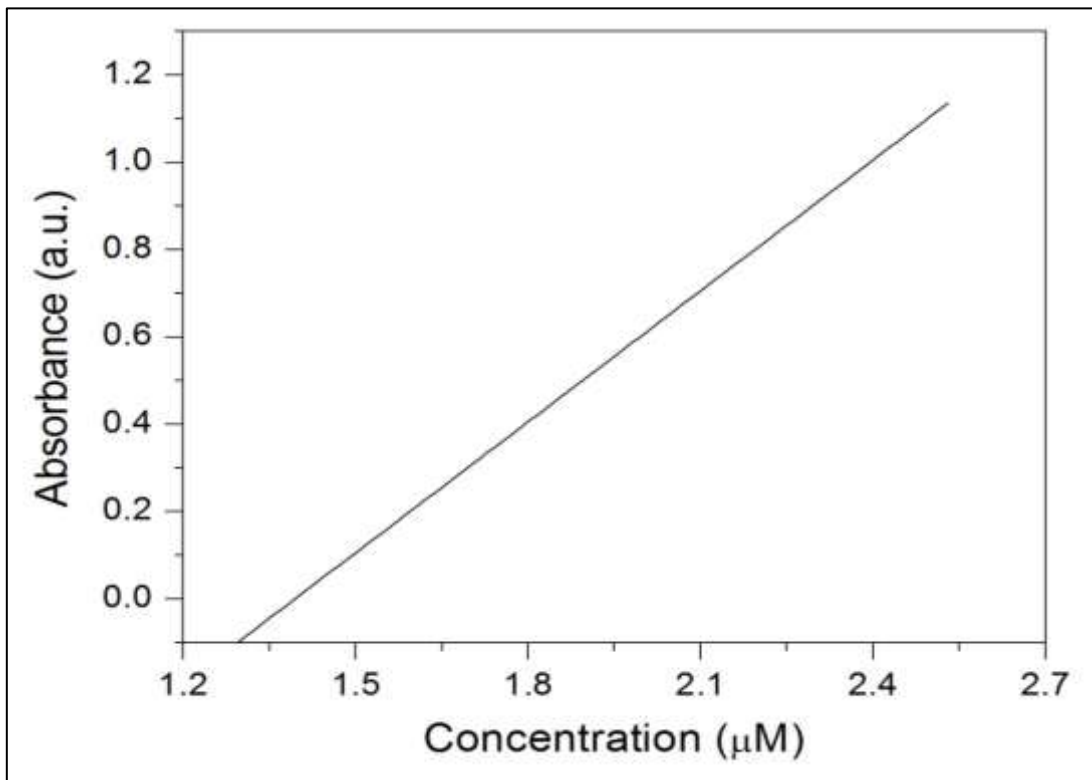
Figure (4.8): Absorbance versus dye concentration.

4.5 Effect of the pH of the dye solution on the DSSCs performance

4.5.1 Experiment

The effect of changing the pH of the dye solutions on the performance of the DSSCs was investigated by treating eosin Y dye solutions with three different acids, where the original pH of eosin Y dissolved in ethanol was around 3.3 measured by the pH meter. Solutions of phosphoric acid (H_3PO_4), hydrochloric acid (HCl) and nitric acid (HNO_3), all of molarity 0.1 M, were added gradually to eosin Y solutions to get solutions of three different pH values ranged from 2.6 to 1.2 in which the TiO_2 films were immersed for 3 hours.

4.5.2 Results and Discussion

4.5.2.1 J-V Characterization of DSSCs after treating the dye with phosphoric acid

The J-V characteristics of DSSCs sensitized with eosin Y at different pH values after the treatment with phosphoric acid is shown in figure (4.9). The pH of 3.3 is referred to the untreated dye solution resulted in a short circuit current density (J_{SC}) of 0.82 mA/cm^2 and an open circuit voltage (V_{OC}) of 0.46 V. By decreasing the pH of the dye solution, the J_{SC} of the DSSC was increased while the V_{OC} was decreased. Figure (4.10) shows the power of the resulting DSSCs as a function of the photo-voltage.
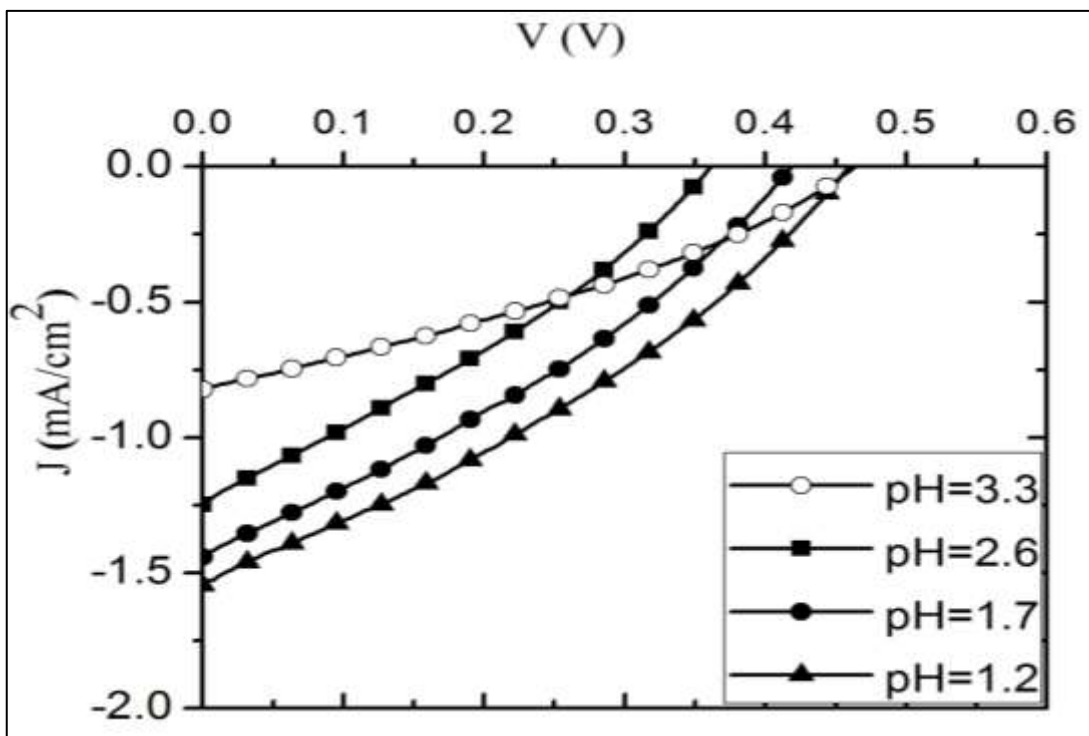
Figure (4.9): Current density (J) versus voltage (V) characteristic curves for DSSCs sensitized with eosin Y solutions of various pH values using phosphoric acid.
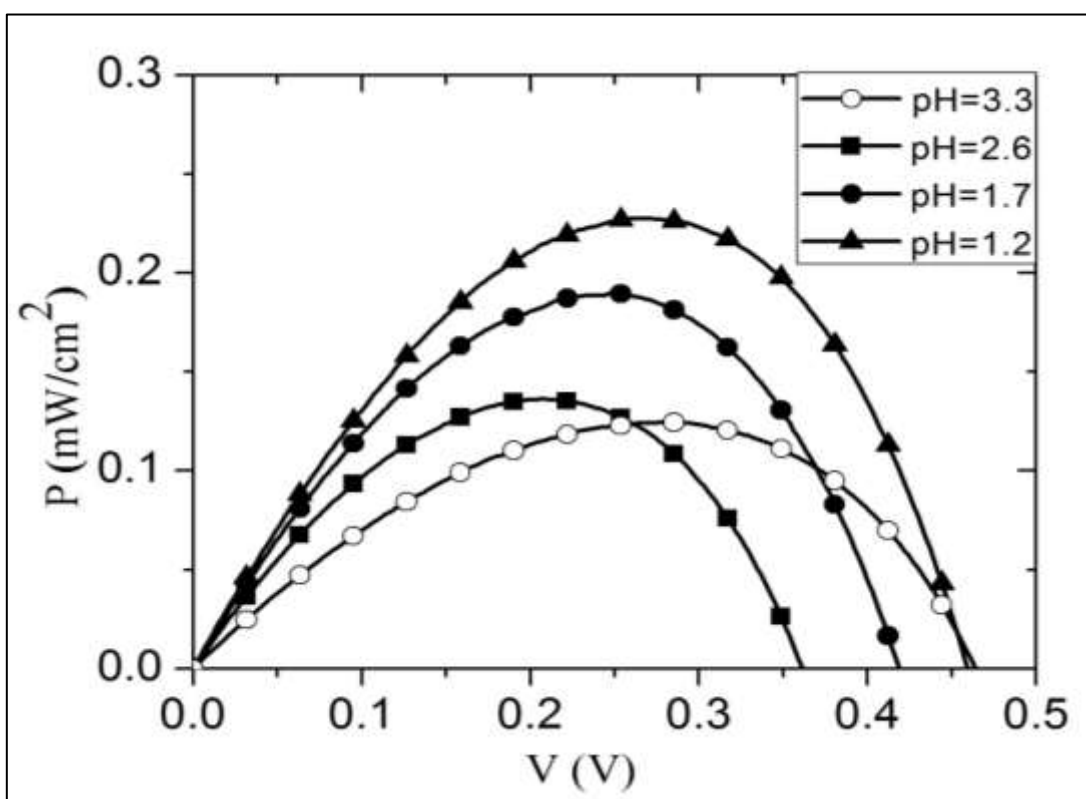
Figure (4.10): Power (P) versus voltage (V) characteristic curves for DSSCs sensitized with eosin Y solutions of various pH values using phosphoric acid.

The photovoltaic parameters of the DSSCs sensitized with eosin Y treated with phosphoric acid is summarized in table (4.2), which shows that the efficiency of the untreated DSSCs is 0.12% while the efficiency of the DSSCs treated with phosphoric acid has found to increase gradually to reach 0.22%. This means that efficiency of the assembled DSSCs was increased by percentage of 0.83% when the pH of the dye solution was 1.2.

Table (4.2): Photovoltaic parameters of the DSSCs sensitized by eosin Y at different pH values using phosphoric acid (H_3PO_4).

pH values	J_{SC} (mA/cm^2)	V_{OC} (V)	J_m (mA/cm^2)	V_m (V)	FF	η %
3.3	0.82	0.460	0.43	0.290	0.33	0.12
2.6	1.24	0.360	0.59	0.222	0.29	0.13
1.7	1.43	0.411	0.72	0.250	0.30	0.18
1.2	1.54	0.455	0.81	0.270	0.31	0.22

4.5.2.2 J-V Characterization of DSSCs after treating the dye with hydrochloric acid (HCl)

The J-V characteristics of DSSCs sensitized with eosin Y at different pH values after the treatment with hydrochloric acid (HCl) is shown in figure (4.11). The untreated dye solution resulted in a short circuit current density (J_{SC}) of 0.82 mA/cm^2 and an open circuit voltage (V_{OC}) of 0.46 V. By decreasing the pH of the dye solution, the J_{SC} of the DSSC was increased to 1.41 mA/cm^2 at the pH of 1.3 while the V_{OC} at that pH was decreased to 0.41 V. Figure (4.12) shows the power as a function of the photo-voltage.

Figure (4.11): Current density (J) versus voltage (V) characteristic curve for DSSCs sensitized with eosin Y solutions at various pH values using hydrochloric acid.
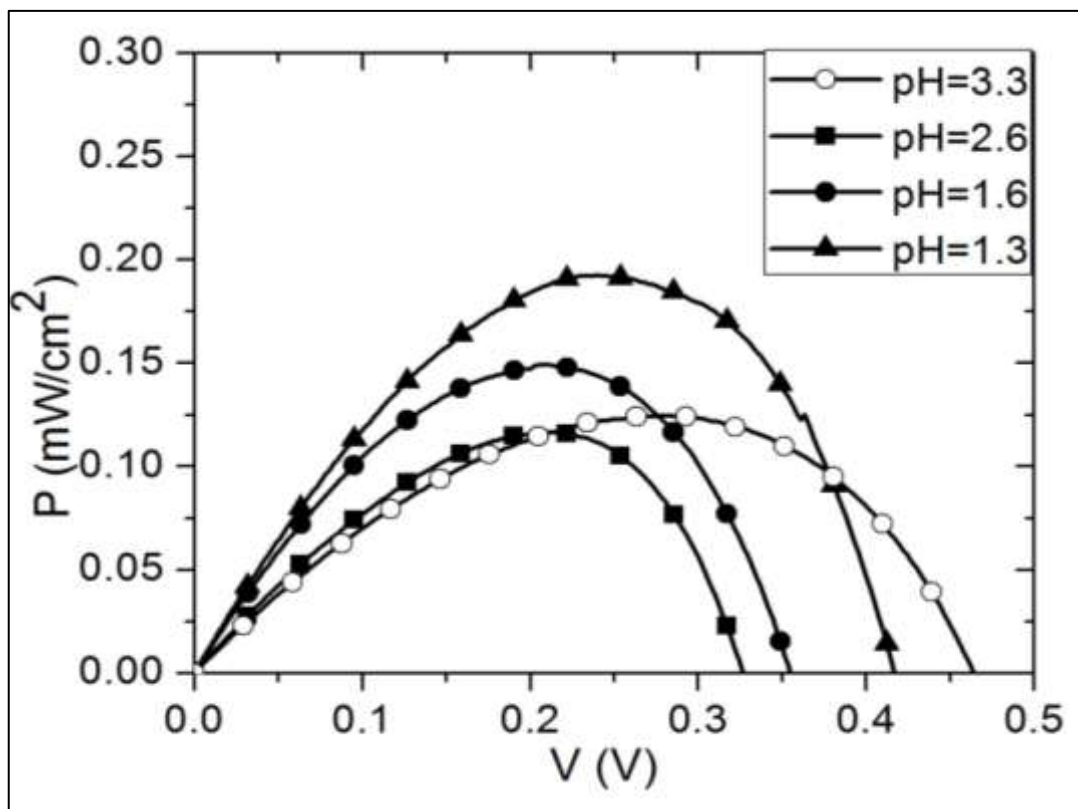
Figure (4.12): Power (P) versus voltage (V) characteristic curves for DSSCs sensitized with eosin Y dye solutions of various pH values using hydrochloric acid.
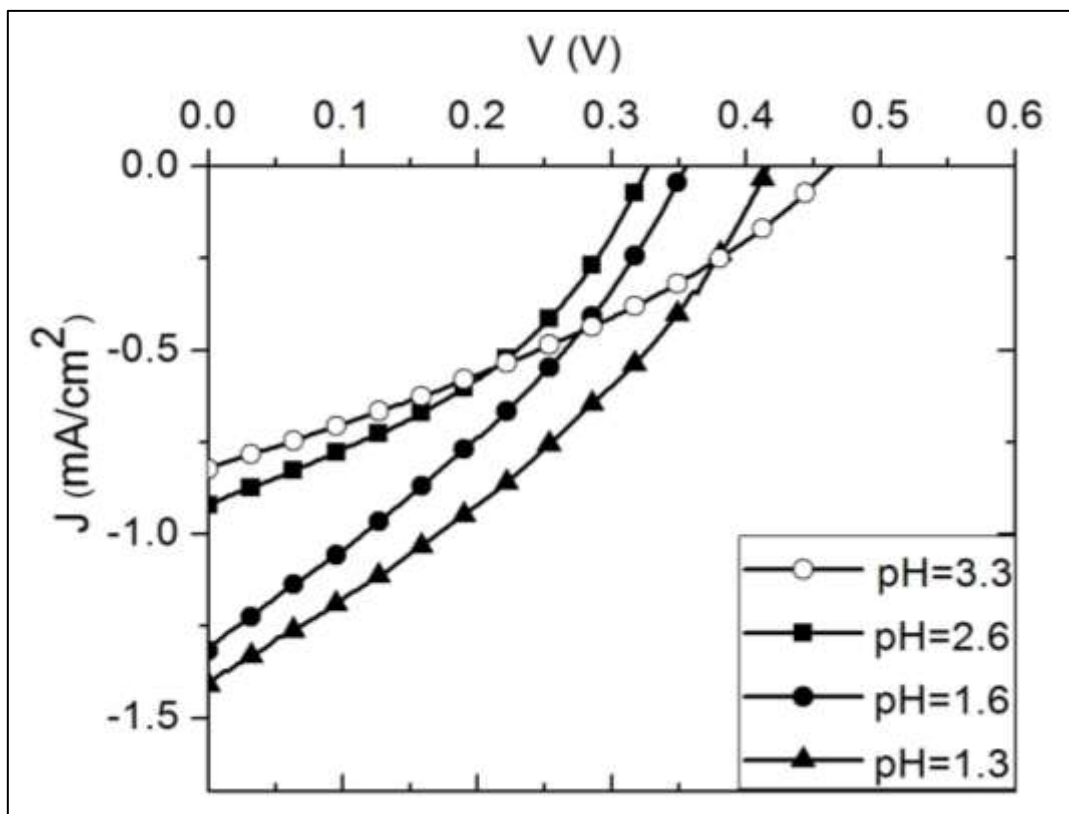
Table (4.3) shows the photovoltaic parameters of the DSSCs sensitized with eosin Y treated with hydrochloric acid, where the efficiency (η) of the DSSCs is found to increase from 0.12% at pH of 3.3 to 0.19% at pH of 1.3.

Table (4.3): Photovoltaic parameters of the DSSCs sensitized by eosin Y at different pH values using hydrochloric acid.

pH values	J_{SC} (mA/cm^2)	V_{OC} (V)	J_m (mA/cm^2)	V_m (V)	FF	η %
3.3	0.82	0.460	0.43	0.290	0.33	0.12
2.6	0.94	0.324	0.50	0.221	0.36	0.12
1.6	1.30	0.355	0.67	0.220	0.32	0.15
1.3	1.41	0.410	0.75	0.253	0.33	0.19

4.5.2.3 J-V Characterization of DSSCs after treating the dye with nitric acid (HNO₃)

Figure (4.13) shows the J-V characteristics of DSSCs sensitized with eosin Y at different pH values after the treatment with nitric acid (HNO₃). According to that figure, decreasing the pH of the dye solution resulted in an increase of the J_{SC} of the DSSC. The power of the resulting DSSCs as a function of voltage is shown (4.14).

Figure (4.13): Current density (J) versus voltage (V) characteristic curve for DSSCs sensitized with eosin Y solutions at various pH values using nitric acid.
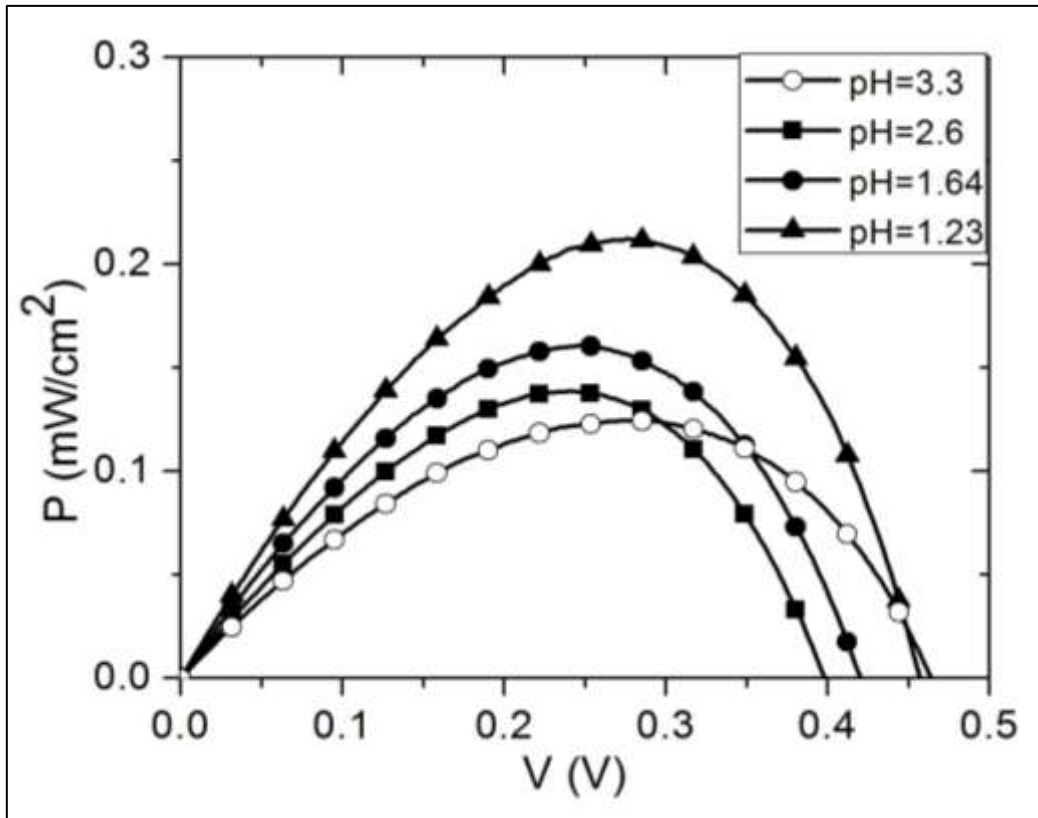
Figure (4.14): Power (P) versus voltage (V) characteristic curves for DSSC sensitized with eosin Y dye solutions of various pH values using nitric acid.

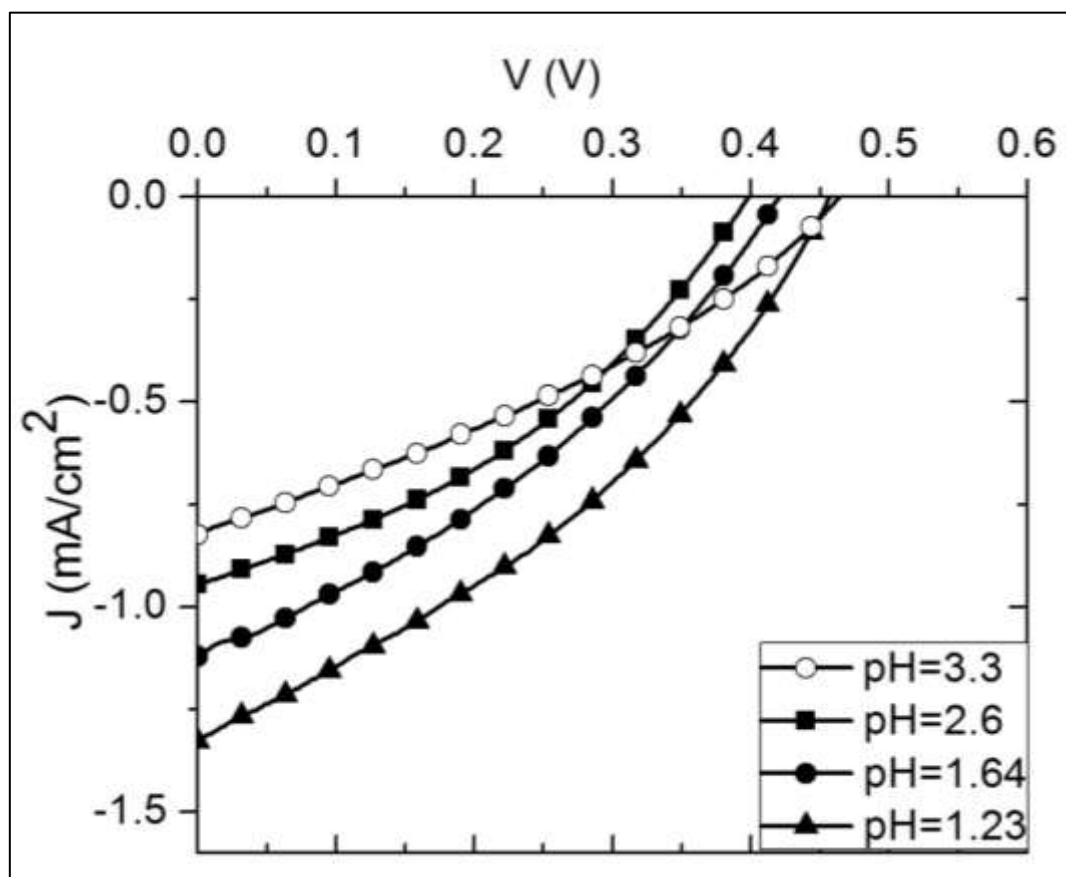The photovoltaic parameters of the DSSCs sensitized with eosin Y treated with nitric acid is presented in table (4.4), where the efficiency (η) of the DSSCs was found to increase gradually from 0.12% to 0.21% at pH of 1.23, so, the efficiency was increased by 0.75%.

Table (4.4): Photovoltaic parameters of the DSSCs sensitized by eosin Y at different pH values using nitric acid.

pH values	J_{SC} (mA/cm^2)	V_{OC} (V)	J_m (mA/cm^2)	V_m (V)	FF	η %
3.3	0.82	0.460	0.43	0.290	0.33	0.12
2.6	0.94	0.395	0.53	0.250	0.35	0.13
1.64	1.11	0.419	0.63	0.254	0.34	0.16
1.23	1.32	0.455	0.76	0.279	0.35	0.21

4.6 Using eosin Y derivative in dyeing the TiO_2 films

4.6.1 Experiment

To investigate the effect of using other derivatives of eosin Y in dyeing the TiO_2 films, a mixture of phenylhydrazine hydrochloride solution and eosin Y solution was prepared in the manner mentioned in section 3.2.7. TiO_2 films were dyed with the resulting mixture for 3 hours. After assembling the DSSCs, the photovoltaic parameters were investigated by the I-V measurement system.

4.6.2 Results and discussion

4.6.2.1 Absorption spectrum

The absorption spectrum of eosin Y derivative (eosin Y with phenylhydrazine hydrochloride) dissolved in ethanol and that of the TiO_2 electrode after being soaked in the dye solution is shown in figure (4.15). The absorption spectrum of the eosin Y derivative in ethanol shows a main peak at a wavelength of 535 nm, while the absorption spectrum of eosin Y derivative/TiO_2 has a main peak at wavelength of 527.5 nm.
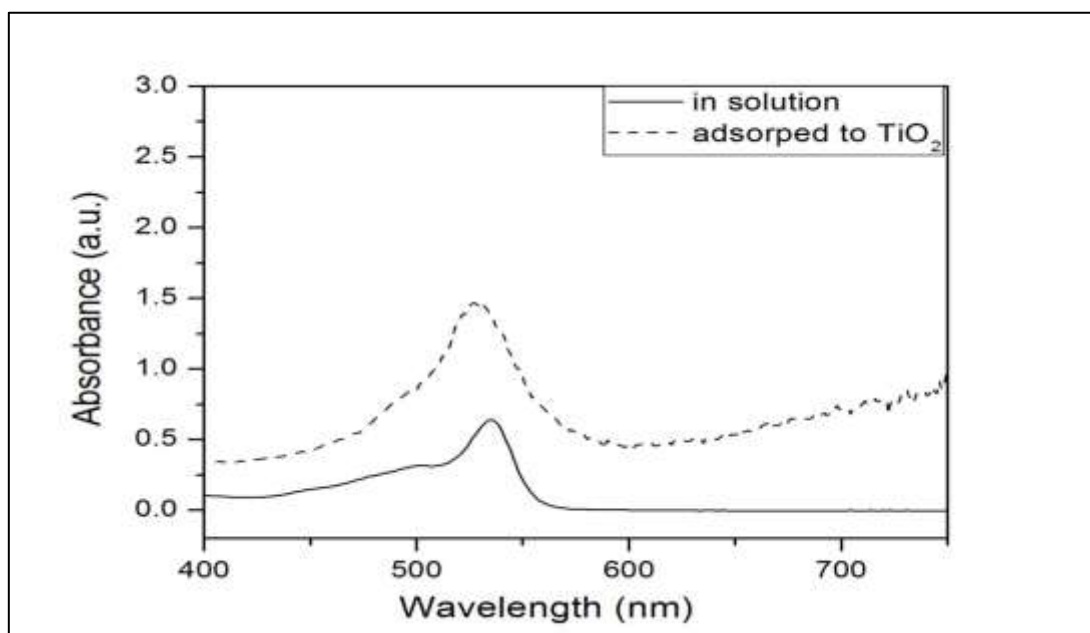
Figure (4.15): Absorption spectrum of eosin Y derivative in ethanol solution and of eosin Y derivative adsorbed onto TiO_2 film.

4.6.2.2   J-V Characterization of DSSCs sensitized by eosin Y derivative

The J–V characteristics of DSSCs dyed with eosin Y derivative solution is shown in figure (4.16). The short circuit current density (J_{SC}) of the DSSCs dyed with eosin Y derivative solution was 1.25 mA/cm^2 and the open circuit voltage (V_{OC}) was 0.412 V. While the I_{SC} of the DSSCs dyed with eosin Y solution was 0.82 mA/cm^2 and the V_{OC} was 0.46 V. The fill factor (FF) of the DSSCs dyed with eosin Y derivative solution was 0.47 while the fill factor of the DSSCs dyed with eosin Y solution without any additives was 0.33.

The power conversion efficiency (η) of the DSSCs sensitized with eosin Y derivative was 0.16%, which is higher than the efficiency of the DSSCs without any additives, where the efficiency was improved by 0.33%.

The power of the resulting DSSCs as a function of voltage is shown in figure (4.17).
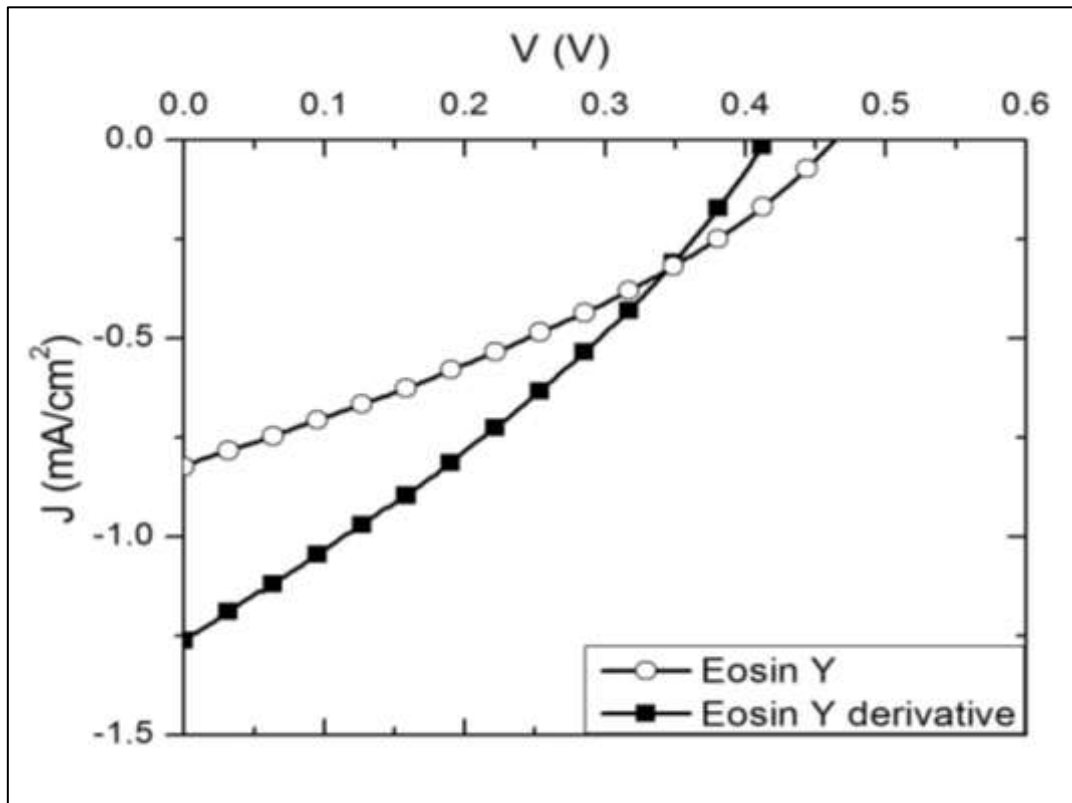
Figure (4.16): Current density (J) versus voltage (V) characteristic curves for DSSCs dyed with eosin Y solution and with eosin Y derivative solution.
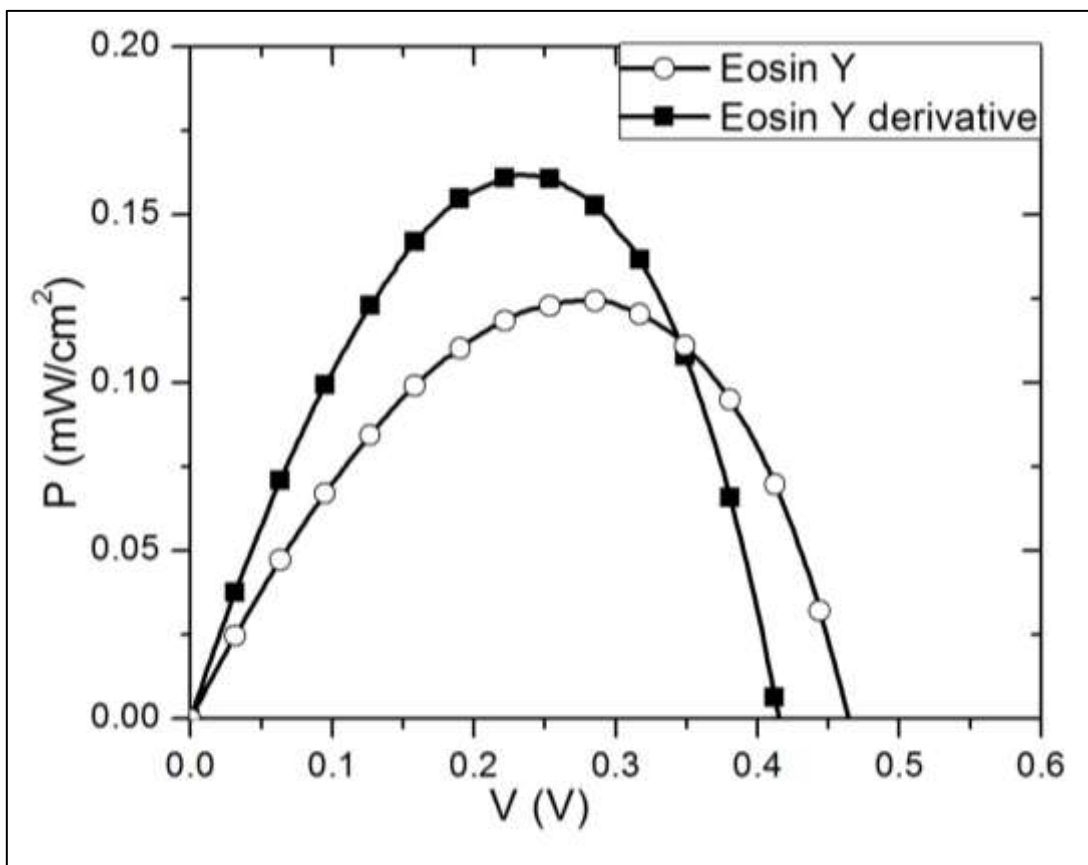
Figure (4.17): Power (P) versus voltage (V) characteristic curves for DSSCs dyed with eosin Y solution and with eosin Y derivative solution.

4.7   Effect of adding ZnO upper layers on the DSSCs performance

One of the methods used to prevent the injected electrons in the TiO_2 electrode from recombining with both the oxidized dye and the tri-iodide in the electrolyte is adding a blocking layer at the TiO_2/electrolyte interface. In this section, ZnO layers were used to form an upper blocking layers on the TiO_2 films.

4.7.1   Experiment

Solutions of four different concentrations were prepared from zinc nitrate hexahydrate ($Zn(NO_3)_2$. $6H_2O$) and ethanol, where the concentrations of the resulting solutions were 0.025 M, 0.05 M, 0.1 M and 0.2 M. These solutions were used as precursor solutions in which the TiO_2 films were immersed as mentioned before in section 3.2.8.

4.7.2   J-V Characterization of DSSCs modified with ZnO upper layers

The J–V characteristics of DSSC after adding an upper layer of ZnO as a blocking layer is shown in figure (4.18). The figure compares between the J–V characteristics of the DSSCs without adding the ZnO layer and the J–V characteristics of the DSSCs modified with ZnO upper layers, where the concentrations of the precursor solutions used in preparing the ZnO layers were 0.025 M, 0.05 M, 0.1 M and 0.2 M.
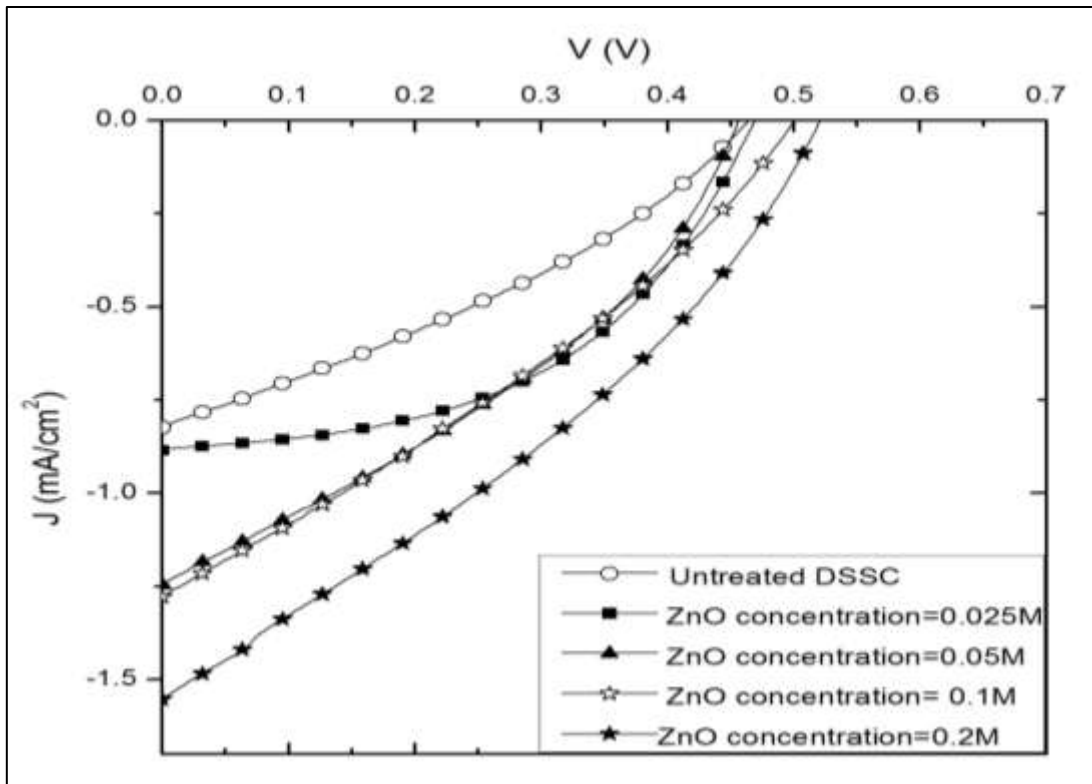
Figure (4.18): Current density (J) versus voltage (V) characteristic curves for DSSCs modified with ZnO upper layer with concentrations of precursor solutions are: 0.025 M, 0.05 M, 0.1 M and 0.2 M.

The short circuit current density (J_{SC}) of the untreated DSSC was 0.82 mA/cm^2 and the open circuit voltage (V_{OC}) was 0.46 V. By increasing the concentration of the precursor solutions, the J_{SC} was increased gradually to reach 1.55 mA/cm^2 at concentration of 0.2 M and the V_{OC} was also increased to 0.519 V at the same concentration.

Table (4.5) shows the main photovoltaic parameters of the modified DSSCs, where the efficiency of the DSSCs increased gradually from 0.20% to 0.26%. The untreated DSSCs has an efficiency of 0.12%. By introducing a ZnO layer of concentration 0.2M, the efficiency was improved by 1.16%.

Increasing the concentration of the precursor solution results in more ZnO molecules to be adsorbed onto the TiO_2 films and so a more compact layer that acts as a blocking layer at the TiO_2/electrolyte interface. This blocking layer can suppress the electrons from recombining with both the oxidized dye and the tri-iodide in the electrolyte, which contributes in improving the efficiency of the DSSCs.

Table (4.5): Potovoltaic parameters of the DSSCs modified with ZnO upper layer.

ZnO concentration (M)	J_{SC} (mA/cm^2)	V_{OC} (V)	J_m (mA/cm^2)	V_m (V)	FF	η %
0.025	0.88	0.468	0.62	0.320	0.48	0.20
0.05	1.24	0.454	0.66	0.297	0.35	0.19
0.1	1.27	0.498	0.66	0.297	0.31	0.19
0.2	1.55	0.519	0.83	0.311	0.32	0.26

The power of the resulting DSSC as a function of voltage is shown in figure (4.19).

Figure (4.19): Power (P) versus voltage (V) characteristic curves for DSSCs modified with ZnO upper layer with concentrations of precursor solutions are: 0.025 M, 0.05 M, 0.1 M and 0.2 M.

4.8   Effect of adding ZnO under-layers on the DSSCs performance

4.8.1   Experiment

Solutions of four different concentrations were prepared from zinc nitrate hexahydrate ($Zn(NO_3)_2$. $6H_2O$) and ethanol, where the concentrations of the resulting solutions were 0.025 M, 0.05 M, 0.1 M and 0.2 M. These solutions were used as precursor solutions in which the FTO glass substrates were immersed as mentioned before in section 3.2.8.

4.8.2   J-V Characterization of DSSCs with adding ZnO under-layers

The J–V characteristics of DSSC after adding an under layer of ZnO as a blocking layer is shown in figure (4.20). The short circuit current density (J_{SC}) of the untreated DSSC was 0.82 mA/cm^2 and the open circuit voltage (V_{OC}) was 0.46 V. By

increasing the concentration of the precursor solutions, the J_{SC} was decreased to reach 0.05 mA/cm^2 at concentration of 0.2 M and the V_{OC} was also decreased to 0.310 V at the same concentration.

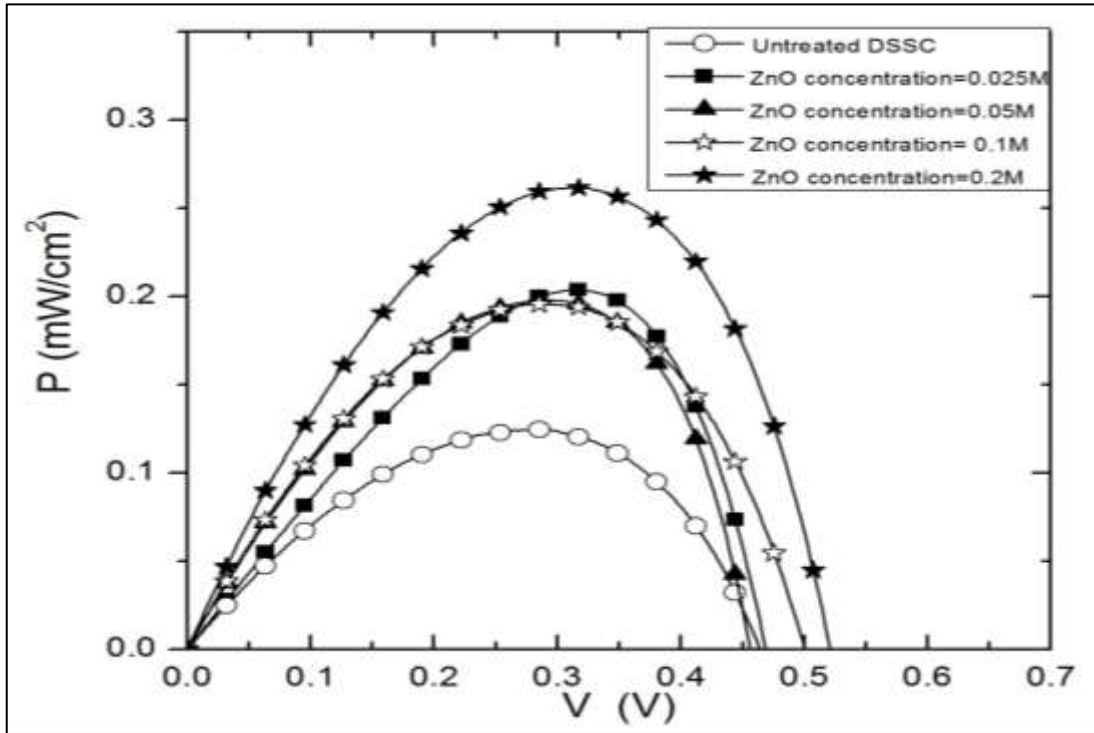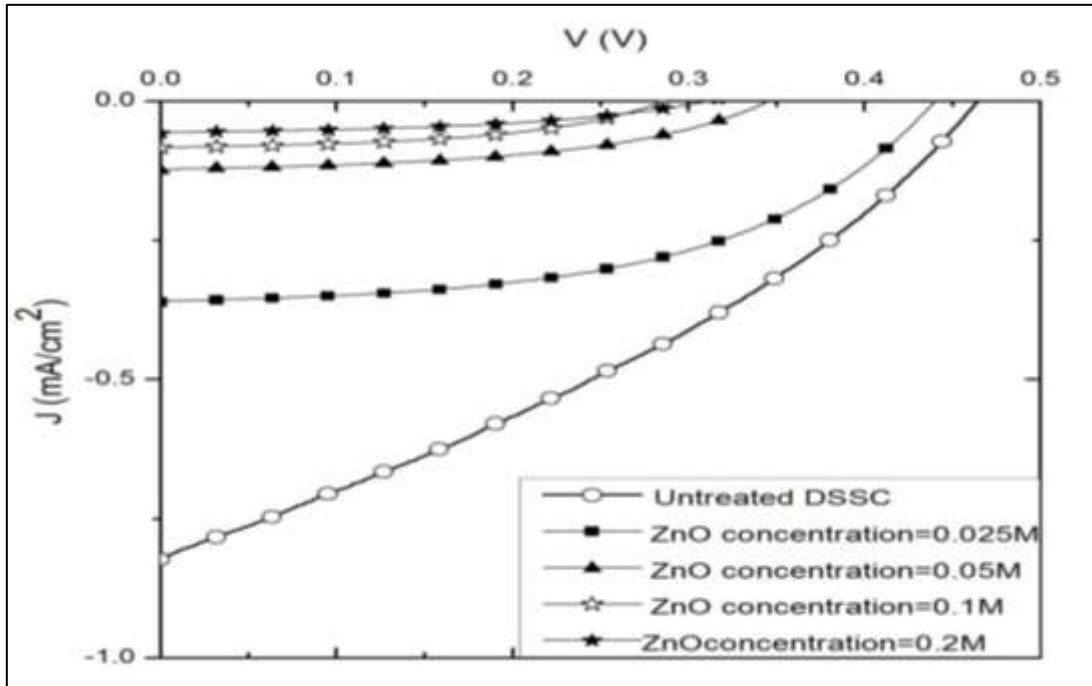**Figure (4.20):** Current density (J) versus voltage (V) characteristic curves for DSSCs modified with ZnO under layer with concentrations of precursor solutions are 0.025 M, 0.05 M, 0.1 M and 0.2 M.

Table (4.6) shows the main photovoltaic parameters of the modified DSSCs, where the fill factor has decreased with increasing the ZnO concentration from 0.52 at ZnO concentration of 0.025 M to 0.40 at ZnO concentration of 0.2M.

Table (4.6): Photovoltaic parameters of the DSSCs with the ZnO under layer.

ZnO concentration (M)	J_{SC} (mA/cm^2)	V_{OC} (V)	J_m (mA/cm^2)	V_m (V)	FF	η %
0.025	0.35	0.436	0.26	0.307	0.52	0.08
0.05	0.12	0.343	0.08	0.236	0.45	0.02
0.1	0.08	0.282	0.05	0.196	0.43	0.01
0.2	0.05	0.310	0.03	0.208	0.40	0.007

The efficiency of untreated DSSCs is 0.12%, while the efficiency of the DSSCs treated with ZnO layers is 0.007% at ZnO concentration of 0.2M, which means that the efficiency has dropped drastically by that modification. This drop in the efficiency can be explained as follow: the conduction band edge of the TiO_2 is -4.21 eV and the conduction band edge of the ZnO is -4.1 eV, the existence of the ZnO layer under the TiO_2 layer prevents the electrons from reaching the front electrode, because the conduction band edge of the ZnO is higher than that of the TiO_2 and the electrons need to jump through that energy barrier. So, both the photo-current of the assembled DSSC and the efficiency are usually small. Table (4.6) shows that increasing the ZnO concentration results in more dropped efficiency, since increasing the ZnO concentration means a more compact layer of the ZnO. So, the electrons can't overcome that barrier and reach the front electrode.

The power of the resulting DSSC as a function of voltage is shown in figure (4.21).
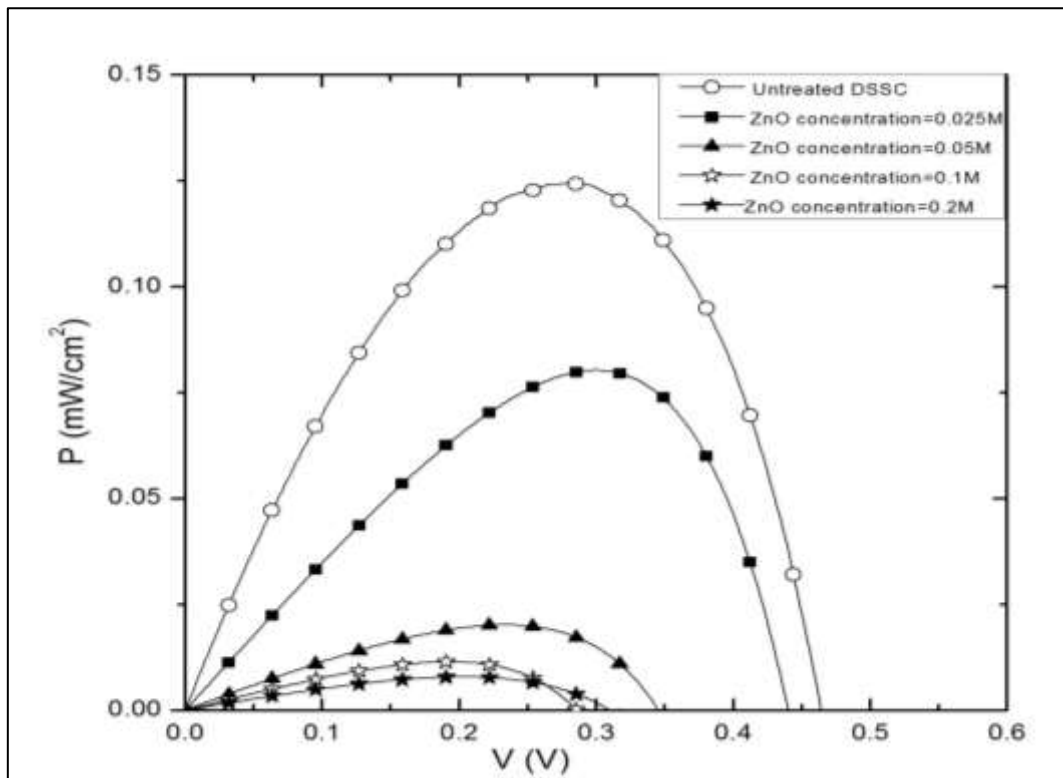
Figure (4.21): Power (P) versus voltage (V) characteristic curves for DSSCs modified with ZnO under layer with concentrations of precursor solutions are 0.025 M, 0.05 M, 0.1 M and 0.2 M.

Chapter 5
Conclusions

Chapter 5
Conclusion

5.1 Conclusions

The objective of the thesis work was to enhance the efficiency of the DSSCs by some modifications such as changing the dyeing duration of TiO_2 films, preparing a derivative of eosin Y solution is used as a new photosensitizer, changing the pH of the dye solution and adding ZnO blocking layers.

The periods of 1 hour, 3 hours, 6 hours and 24 hours were studied. The results showed that the short circuit current density (J_{SC}) and the open circuit voltage (V_{OC}) have their maximum values when the dyeing duration was 3 hours, where the J_{SC} was 0.82 mA/cm^2 and the V_{OC} was 0.46 V.

The optical properties of the dye solution were characterized by UV-Vis spectroscopy and the main photovoltaic parameters were calculated by analyzing data resulted from the I-V measurement system. The absorption spectrum of eosin Y dissolved in ethanol showed a main peak at wavelength of 525nm, while the peak of eosin Y derivative was at 535nm, which means that the peak was shifted to a longer wavelength when a derivative of eosin Y was used.

The dye solution was modified by preparing a mixture of phenylhydrazine hydrochloride solution and eosin Y solution, which was known as eosin Y derivative. When the eosin Y derivative was used as a photo-sensitizer in the DSSCs, the J_{SC} was 1.25 mA/cm^2 and V_{OC} was 0.412 V. In addition, the efficiency was improved by 0.33%.

Effect of changing the pH value of the dye solution was studied by using phosphoric, hydrochloric and nitric acids. The results showed that decreasing the pH of the dye solution can enhance the efficiency of the DSSCs, where the efficiency increased from 0.12% to 0.22% at the pH of 1.2 when the phosphoric acid was added.

The mechanism used in suppressing the recombination of injected electrons with both the redox electrolyte and the oxidized dye was adding ZnO blocking layers which were introduced as upper and under layers. For the ZnO upper layers, the J_{SC} and the V_{OC} of the assembled DSSCs have increased gradually by increasing the concentration of the ZnO, where the Jsc was 1.55 mA/cm^2 and the V_{OC} was 0.519V at ZnO concentration of 0.2M. The efficiency was improved by 1.16% at that concentration of ZnO.

The under-layers resulted in a drop of the J_{SC}, the V_{OC} and the efficiency, when the concentration of the ZnO was increased.

DSSCs are considered a new promising route toward simple fabrication, low-cost, environment friendly power generation, as a clean photoelectric conversion system and potential alternative to the traditional photovoltaic devices. All these reasons make the field of DSSCs a preferable research field in which great efforts have been taken to improve the efficiency of DSSCs.

References

References:

Abu-Jasser, A. (2010). A stand-alone photovoltaic system, case study: a residence in Gaza. *Journal of Applied Sciences in Environmental Sanitation*, *5*(1), 81-91.

Adib, R. (2015). *Renewables 2015 Global Status Report*. Retrieved 12 July, 2016, from : www.ren21.net/wp-content/uploads/2015/.../REN12-GSR2015_Onlinebook_low1.pdf

Aribisala, H. A. (2013). Improving the efficiency of solar photovoltaic power system. (Master's thesis). Retrieved August 6, 2016, from: http://digitalcommons.uri.edu/theses/161

Brinker, D. J., Curtis, H. B., Flood, D. J., Jenkins, P., & Scheiman, D. A. (1996). A Summary of the International Workshops on Space Solar Cell Calibration and Measurement Techniques. In *NASA CONFERENCE PUBLICATION* (pp. 186-190). NASA.

Cahen, D., Grätzel, M., Cuillemoles, J., & Hodes, G. (2001). Dye-sensitized solar cells: principles of operation. *Electrochemistry of Nanomaterials*, *7*, 201-219.

Cahen, D., Hodes, G., Grätzel, M., Guillemoles, J. F., & Riess, I. (2000). Nature of photovoltaic action in dye-sensitized solar cells. *The Journal of Physical Chemistry B*, *104*(9), 2053-2059.

Chen, C. J. (2011). *Physics of solar energy*. John Wiley & Sons.

Chou, C. S., Chou, F. C., & Kang, J. Y. (2012). Preparation of ZnO-coated TiO_2 electrodes using dip coating and their applications in dye-sensitized solar cells. *Powder Technology*, *215*, 38-45.

Chou, C. S., Yang, R. Y., Yeh, C. K., & Lin, Y. J. (2009). Preparation of TiO_2/nano-metal composite particles and their applications in dye-sensitized solar cells. *Powder Technology*, *194*(1), 95-105.

Das, P., Roy, A., Das, S., & Devi, P. (2016). Enhanced stability of Zn_2SnO_4 with N719, N3 and eosin Y dye molecules for DSSC application. *Physical Chemistry Chemical Physics*, *18*(3), 1429-1438.

Fredin, K. (2007). Studies of charge transport processes in dye-sensitized solar cells. (Doctoral dissertation). Retrieved July 15, 2016, from: http://kth.diva-portal.org/smash/get/diva2:12288/FULLTEXT01.pdf

Galvez, J. B., & Rodriguez, S. M. (2003). Solar Detoxification Technology. *Solar Detoxification; UNESCO Publishing: Paris*, 117.

Gerischer, H., Michel-Beyerle, M. E., Rebentrost, F., & Tributsch, H. (1968). Sensitization of charge injection into semiconductors with large band gap. *Electrochimica Acta*, *13*(6), 1509-1515.

Goetzberger, A., & Hebling, C. (2000). Photovoltaic materials, past, present, future. *Solar energy materials and solar cells*, *62*(1), 1-19.

Gong, J., Liang, J., & Sumathy, K. (2012). Review on dye-sensitized solar cells (DSSCs): fundamental concepts and novel materials. *Renewable and Sustainable Energy Reviews*, *16*(8), 5848-5860.

Grätzel, M. (2001). Photoelectrochemical cells. *Nature*, *414*(6861), 338-344.

Green, M. A. (1982). *Solar cells: operating principles, technology, and system applications*. Prentice-Hall, Inc., Englewood Cliffs, NJ, United States.

Green, M. A. (2007). Thin-film solar cells: review of materials, technologies and commercial status. *Journal of Materials Science: Materials in Electronics*, *18*(1), 15-19.

Green, M. A., Emery, K., Hishikawa, Y., & Warta, W. (2010). Solar cell efficiency tables (version 36). *Progress in photovoltaics: research and applications*, *18*(5), 346-352.

Hagfeldt, A., & Grätzel, M. (1995). Light-induced redox reactions in nanocrystalline systems. *Chemical Reviews*, *95*(1), 49-68.

Hagfeldt, A., Boschloo, G., Sun, L., Kloo, L., & Pettersson, H. (2010). Dye-sensitized solar cells. *Chemical reviews*, *110*(11), 6595-6663.

Halme, J. (2002). Dye-sensitized nanostructured and organic photovoltaic cells: technical review and preliminary tests. (Unpublished Master's thesis). Helsinki university of technology, Finland.

Hegedus, S. S., & Luque, A. (2003). Status, trends, challenges and the bright future of solar electricity from photovoltaics. *Handbook of photovoltaic science and engineering*, John Wiley & Sons, 1-43 .

Hosenuzzaman, M., Rahim, N. A., Selvaraj, J., Hasanuzzaman, M., Malek, A. B. M. A., & Nahar, A. (2015). Global prospects, progress, policies, and environmental impact of solar photovoltaic power generation. *Renewable and Sustainable Energy Reviews*, *41*, 284-297.

Huang, S. Y., Schlichthörl, G., Nozik, A. J., Grätzel, M., & Frank, A. J. (1997). Charge recombination in dye-sensitized nanocrystalline TiO_2 solar cells. *The Journal of Physical Chemistry B*, *101*(14), 2576-2582.

Ito, S., Murakami, T. N., Comte, P., Liska, P., Grätzel, C., Nazeeruddin, M. K., & Grätzel, M. (2008). Fabrication of thin film dye sensitized solar cells with solar to electric power conversion efficiency over 10%. *Thin solid films*, *516*(14), 4613-4619.

Jacobson, M. Z., & Delucchi, M. A. (2011). Providing all global energy with wind, water, and solar power, Part I: Technologies, energy resources, quantities and areas of infrastructure, and materials. *Energy policy*, *39*(3), 1154-1169.

Jäger, K., Isabella, O., Smets, A., Van Swaaij, R. A. C. M. M., & Zeman, M. (2014). Solar Energy-Fundamentals, Technology, and Systems. *Delft University of Technology*, *77*, 78.

Kandavelu, V., Huang, H. S., Jian, J. L., Yang, T. C. K., Wang, K. L., & Huang, S. T. (2009). Novel iminocoumarin dyes as photosensitizers for dye-sensitized solar cell. *Solar Energy*, *83*(4), 574-581.

Karlsson, K. M. (2011). *Design, Synthesis and Properties of Organic Sensitizers for Dye Sensitized Solar Cells*. (Ph.D. dissertation). Retrieved July 15, 2016, from: https://www.diva-portal.org/smash/get/diva2:413894/FULLTEXT01.pdf

Khan, M. I. (2013). *A Study on the Optimization of Dye-Sensitized Solar Cells*. (Master's thesis). Retrieved July 15, 2016, from: http://scholarcommons.usf.edu/etd/4519

Kuciauskas, D., Freund, M. S., Gray, H. B., Winkler, J. R., & Lewis, N. S. (2001). Electron transfer dynamics in nanocrystalline titanium dioxide solar cells sensitized with ruthenium or osmium polypyridyl complexes. *The Journal of Physical Chemistry B*, *105*(2), 392-403.

Kuzmych, O. (2014). Development and characterization of dye- and semiconductor sensitized solar cells based on structurally organized titanium dioxide. (Ph.D. dissertation). Retrieved September 15, 2016, from: https://depotuw.ceon.pl/handle/item/699

Lee, K. M., Chiu, W. H., Wei, H. Y., Hu, C. W., Suryanarayanan, V., Hsieh, W. F., & Ho, K. C. (2010). Effects of mesoscopic poly (3, 4-ethylenedioxythiophene) films as counter electrodes for dye-sensitized solar cells. *Thin Solid Films*, *518*(6), 1716-1721.

Mathew, S., Yella, A., Gao, P., Humphry-Baker, R., Curchod, B. F., Ashari-Astani, N., & Grätzel, M. (2014). Dye-sensitized solar cells with 13% efficiency achieved through the molecular engineering of porphyrin sensitizers. *Nature chemistry*, *6*(3), 242-247.

Meyer-Arendt, Jürgen, R. (1989). *Introduction to classical and modern optics. Englewood Cliffs*.(3rd ed). Prentice-Hall.

Nazeeruddin, M. K., Kay, A., Rodicio, I., Humphry-Baker, R., Müller, E., Liska, P., & Grätzel, M. (1993). Conversion of light to electricity by cis-X2bis (2, 2'-bipyridyl-4, 4'-dicarboxylate) ruthenium (II) charge-transfer sensitizers (X= Cl-, Br-, I-, CN-, and SCN-) on nanocrystalline titanium dioxide electrodes. *Journal of the American Chemical Society*, *115*(14), 6382-6390.

Nazeeruddin, M. K., Pechy, P., Renouard, T., Zakeeruddin, S. M., Humphry-Baker, R., Comte, P., ... & Spiccia, L. (2001). Engineering of efficient panchromatic sensitizers for nanocrystalline TiO_2-based solar cells. *Journal of the American Chemical Society*, *123*(8), 1613-1624.

Nelson, J. (2003). *The physics of solar cells*. World Scientific Publishing Co. Inc.

Noumissing Sao, C. (2009). Dye sensitized solar cells based on perylene derivatives. (Doctoral dissertation). Retrieved from https://kobra.bibliothek.uni-kassel.de/bitstream/urn:nbn:de:hebis:34-2009110330833/3/Noumissing-Thesis.pdf

O'Regan, B., & Grätzel, M. (1991). A low-cost, high-efficiency solar cell based on dye-sensitized. *nature*, *353*(6346), 737-740.

Obotowo, I. N., Obot, I. B., & Ekpe, U. J. (2016). Organic sensitizers for dye-sensitized solar cell (DSSC): Properties from computation, progress and future perspectives. *Journal of Molecular Structure*, *1122*, 80-87.

Radwan, I. (2015). *Dye sensitized solar cells based on natural dyes extracted from plant roots*. (Master's thesis). Retrieved July 15, 2016, from: http://library.iugaza.edu.ps/thesis/115517.pdf

Ramasamy, P., Kang, M. S., Cha, H. J., & Kim, J. (2013). Highly efficient dye-sensitized solar cells based on HfO_2 modified TiO_2 electrodes. *Materials Research Bulletin*, *48*(1), 79-83.

Rouessac, F., & Rouessac, A. (2013). *Chemical analysis: modern instrumentation methods and techniques*. John Wiley & Sons.

Ryan, M. (2009). PGM Highlights: ruthenium complexes for dye sensitized solar cells. *Platinum Metals Review*, *53*(4), 216-218.

Shockley, W. (1976). *Electrons and holes in semiconductors, with applications to transistor electronics*. Krieger Pub. Co.

Sima, C., Grigoriu, C., & Antohe, S. (2010). Comparison of the dye-sensitized solar cells performances based on transparent conductive ITO and FTO. *Thin Solid Films*, *519*(2), 595-597.

Tachibana, Y., Moser, J. E., Grätzel, M., Klug, D. R., & Durrant, J. R. (1996). Subpicosecond interfacial charge separation in dye-sensitized nanocrystalline titanium dioxide films. The Journal of Physical Chemistry, *100*(51), 20056-20062.

Tanabe, K. (2009). A review of ultrahigh efficiency III-V semiconductor compound solar cells: multijunction tandem, lower dimensional, photonic up/down conversion and plasmonic nanometallic structures. *Energies*, *2*(3), 504-530.

Toivola, M. (2010). Dye-sensetized solar cells on alternative substrates. (Doctoral dissertation). Retrieved September 2, 2016, from: http://lib.tkk.fi/Diss/2010/isbn9789526030708/

Tolvanen, A. (2003). *Characterization and manufacturing techniques of dye sensitized solar cells*. (Master's thesis) Helisinki University of Technology, Finland.

Yang, F. (2008). Thin film solar cells grown by organic vapor phase deposition. *Dissertation Abstracts International*, *69-07*, Section: B, page: 4348.; 187 p.

Yella, A., Lee, H. W., Tsao, H. N., Yi, C., Chandiran, A. K., Nazeeruddin, M. K., & Grätzel, M. (2011). Porphyrin-sensitized solar cells with cobalt (II/III)–based redox electrolyte exceed 12 percent efficiency. *science*, *334*(6056), 629-634.

Zaban, A., Greenshtein, M., & Bisquert, J. (2003). Determination of the electron lifetime in nanocrystalline dye solar cells by open-circuit voltage decay measurements. *ChemPhysChem*, *4*(8), 859-864.

Zeman, M. (2003). *Introduction to photovoltaic solar energy*. Holland: Delft University of Technology.

Zhang, Q., Dandeneau, C. S., Zhou, X., & Cao, G. (2009). ZnO Nanostructures for Dye-Sensitized Solar Cells. *Advanced Materials*, *21*(41), 4087-4108.